Angular dependence of antiferromagnetic order induced by paramagnetism in a *d*-wave superconductor

Ken-ichi Hosoya and Ryusuke Ikeda
Department of Physics, Graduate School of Science, Kyoto University, Kyoto 606-8502, Japan
(Received 4 June 2013; published 23 September 2013)

Antiferromagnetic (AFM) order and a spatial order peculiar to Fulde-Ferrell-Larkin-Ovchinnikov (FFLO) states, previously indicated in the quasi-two-dimensional d-wave superconductors $CeCoIn_5$ with strong paramagnetic pair breaking (PPB) in a magnetic field parallel to the basal plane, are considered in the field configurations tilted from the basal plane within an approach assuming that the wavelength of the FFLO modulation is relatively long. It is demonstrated that, with increasing the tilt angle, both the AFM and FFLO orders are gradually suppressed, and that disappearance of the AFM order in the zero-temperature limit occurs at a lower angle than that of the FFLO state. Consequently, a *nonmagnetic* FFLO-ordered high-field superconducting phase is realized in an intermediate range of the tilt angle even at low enough temperatures. As the perpendicular field configuration ($\mathbf{H} \parallel c$) is approached by the field tilt, the nonvanishing AFM order in real space tends to occur only close to the FFLO nodal planes in contrast to the high-field behavior in the $\mathbf{H} \perp c$ case. Further, in the field versus temperature (H-T) phase diagram, the AFM order reduces, at a higher angle, to an AFM quantum critical point lying at a *lower* field than $H_{c2}(0)$ as a consequence of competition between the field dependencies of the nesting condition and of PPB. These features of the AFM order and the resulting H-T phase diagram strikingly coincide with those seen in a recent NMR measurement on $CeCoIn_5$ in tilted field configurations.

DOI: 10.1103/PhysRevB.88.094513 PACS number(s): 74.70.Tx, 74.20.Rp, 74.20.Fg, 74.25.Ha

I. INTRODUCTION

Recently, the quasi-two-dimensional (Q2D) heavy-fermion superconductor $CeCoIn_5$ has attracted much attention due to a possible realization of a Fulde-Ferrell-Larkin-Ovchinnikov (FFLO) superconducting (SC) state[1,2] in its high-field low-temperature (HFLT) SC phase.[3] This new SC phase is separated through a second-order transition on $H^*(T)$ from the familiar Abrikosov vortex lattice state and has been examined repeatedly in the field configuration $\mathbf{H} \perp c$ parallel to the SC planes.[4] The experimental fact in $\mathbf{H} \perp c$ that this new SC phase is extremely sensitive to both the magnetic[5] and nonmagnetic[6] impurity dopings implies[7] that, prior to the doping, this phase is spatially *inhomogeneous*. Further, an observed square-root ($\sim \sqrt{H - H^*}$) dependence of the internal field in a NMR measurement[8] has been consistent with the picture[4,9] that the HFLT phase includes a FFLO spatial modulation *parallel* to the field. It should be kept in mind that a similar HFLT phase also appears[3,9,10] in the perpendicular field configuration $\mathbf{H} \parallel c$ over a narrower field range.

On the other hand, neutron scattering measurements in $\mathbf{H} \perp c$ have revealed the existence of an incommensurate AFM order within the HFLT SC phase.[11,12] The detected[11,12] staggered moment $\mathbf{m}$ is parallel to the c axis, and its incommensurate wave vector is parallel to [1,1,0] or [1,−1,0] irrespective of the $\mathbf{H}$ direction. As noted elsewhere,[13,14] this AFM ordering should be closely related to the AFM quantum critical behavior near the mean field SC transition field $H_{c2}(0)$ observed not only in $CeCoIn_5$ in $\mathbf{H} \perp c$ and $\mathbf{H} \parallel c$ (Refs. 15–17), but also in pressured $CeRhIn_5$,[18] $NpPd_5Al_2$,[19] and Ce_2PdIn_8.[20]

It is striking that this high-field AFM order does not appear outside the HFLT phase because conventional theories in zero field suggest that the AFM order is suppressed by a nonvanishing value of the SC excitation gap.[21,22] To explain why, in nonzero magnetic fields, the AFM order favors coexistence with the SC order, several pictures have been proposed so far.[13,14,23–25] The common point of view to these theories is that the AFM order is enhanced by the $d_{x^2-y^2}$-wave[26] pairing symmetry and a strong PPB effect. As will be discussed at the end of this paper, on the other hand, there are crucial differences between those existing theories.

In this work, we focus on the intermediate field configurations connecting between the $\mathbf{H} \perp c$ and $\mathbf{H} \parallel c$ cases, motivated by several experiments performed in magnetic fields tilted from the basal (a-b) plane. Neutron scattering measurements[27] have discovered that the 17° rotation of the field away from the basal plane results in the disappearance of the AFM order and have indicated that the staggered moment $\mathbf{m}$ remains fixed along the c axis while the field is tilted. On the other hand, the magnetostriction experiments[28] and the magnetization measurements[29] have shown that the HFLT phase disappears at a larger angle, 20°, which, by being combined with the neutron result,[27] suggests that the FFLO state with no AFM order is realized in a narrow range of the tilt angle. More recently, NMR data[30] obtained by tilting the field direction from the a-b plane have led to several nontrivial pictures on the HFLT phase. First of all, a separation of the AFM-ordered region from the HFLT phase has been clearly seen even for the 7° rotation: The resulting AFM-ordered region existing only within the HFLT phase is, in the H-T phase diagram, narrower than the region of the HFLT one. As the field direction is tilted further, it is first lost from the *higher* fields and higher-temperature side of the HFLT phase. This disappearance of the AFM order from higher fields suggests that an AFM quantum critical point (QCP) to be realized at a higher angle should lie at a lower field than $H_{c2}(0)$. This seems to be closely related to the experimental fact[16,31] that the apparent AFM QCP in $\mathbf{H} \parallel c$ lies at a lower field than $H_{c2}(0)$. In addition, the NMR data in tilted fields[30] suggest an AFM order lying, in the real space, in the vicinity of the FFLO nodal plane on which the SC order parameter vanishes. This is in contrast to the picture seen in $\mathbf{H} \perp c$ that, at least in higher

fields, the AFM order basically favors a spatial region with a nonvanishing SC order parameter.[8,13,14,32]

In this paper, we develop a theory addressing possible HFLT phases of d-wave superconductors with strong PPB effects in the tilted field configurations by extending the treatments in Refs. 14 and 32. To simplify theoretical analysis and make it easier to understand implication of the obtained results, we have used two kinds of approaches separately to examine the angular dependencies: One is based on deriving the Ginzburg-Landau (GL) mean field free energy, which takes a form of an expansion in the SC order parameter but fully includes both the paramagnetic and orbital pair-breaking effects, from an electronic Hamiltonian for a uniaxial Q2D model superconductor. There, effects of the orbital pair breaking, enhanced by tilting the field direction, on the FFLO and AFM orderings are stressed. The other is the Pauli-limited model based on a tight-binding electronic Hamiltonian in which the resulting SC free energy fully includes the SC order parameter, while the orbital pair breaking is neglected so that the SC order parameter is assumed to be homogeneous in the plane perpendicular to the field. It is found that the phase diagrams we obtain in the tilted field configurations become consistent with the experimentally observed one.[30]

This paper is organized as follows. In Sec. II, we derive the GL mean field free energy by including not only the PPB-induced AFM ordering, but also the orbital pair-breaking effect and primarily explain how the two (AFM and FFLO) orders induced by PPB are affected by the field tilt. In Sec. III, the approach in the Pauli limit for the same issue is explained to discuss angular dependencies of not only the phase diagram, but also the details of the AFM order. In summary, the obtained pictures on angular dependencies of the HFLT phase of $CeCoIn_5$ are discussed, and our theory is compared with others[23–25] focusing on the parallel field case.

II. MICROSCOPIC GINZBURG-LANDAU APPROACH

In this section, the mean field GL free energy for a uniaxial d-wave superconductor will be derived based on a Q2D microscopic Hamiltonian by incorporating both the paramagnetic and the orbital pair-breaking effects and will be used to study how the resulting magnetic phase diagram, in particular the AFM order in the FFLO phase corresponding to the HFLT phase of $CeCoIn_5$, in our theory is affected by the tilt of the applied magnetic field from the basal plane. For simplicity of our analysis, the interaction terms will be treated from the outset in the mean field approximation. Then, our starting electronic Q2D Hamiltonian can be expressed, as given elsewhere,[32] in the form $\mathcal{H} = \mathcal{H}_{\rm kin} + \mathcal{H}_{\rm SC} + \mathcal{H}_{\rm AFM}$, where

$$\mathcal{H}_{\rm kin} = d\sum_{\sigma,j}\int d^2\mathbf{r}_\perp\Big[\big[\psi_j^{(\sigma)}(\mathbf{r}_\perp)\big]^\dagger[\,\xi(-i\nabla_\perp + e\mathbf{A}_\perp) - \sigma I\,] \times \psi_j^{(\sigma)}(\mathbf{r}_\perp) - \frac{J}{2}\big[\big[\psi_j^{(\sigma)}(\mathbf{r}_\perp)\big]^\dagger\psi_{j+1}^{(\sigma)}(\mathbf{r}_\perp) + \text{H.c}\big]\Big], \tag{1}$$

with

$$\psi_j^{(\sigma)}(\mathbf{r}_\perp) = \frac{1}{\sqrt{V}}\sum_{\mathbf{p}}\hat{c}_{\mathbf{p},\sigma}e^{i(\mathbf{p}_\perp\cdot\mathbf{r}_\perp + ip_z dj)}, \tag{2}$$

and the mean field interaction terms on superconductivity $\mathcal{H}_{\rm SC}$ and antiferromagnetism $\mathcal{H}_{\rm AFM}$ will be introduced below. The index j is the label of the SC layers, d is the interlayer distance in the c direction, $\sigma(=\pm1)$ denotes the spin projection, J represents the interlayer hopping integral, $\xi(\mathbf{p})$ is the kinetic energy measured from the Fermi energy μ in the two-dimensional (2D) limit with $\mu > J$, V is the system's volume, and $I = g(\theta)\mu_{\rm B}H$ is the Zeeman energy expressed with the Bohr magneton $\mu_{\rm B}$ and the angle-dependent g factor $g(\theta)$. We shall introduce a uniaxial anisotropy and the resulting angle dependence of the g factor because the real $CeCoIn_5$ shows such a remarkable anisotropy of the magnetic susceptibility.[33] As a model, we assume the form $g(\theta) = \sqrt{g_a^2\cos^2\theta + g_c^2\sin^2\theta}$, where g_j is the g factor for an applied field $\mathbf{H}$ in the j direction, and $g_a = g_b$. The unit $\hbar = c = k_{\rm B} = 1$ will be used throughout this paper. The coordinates $\mathbf{r} = (x,y,z)$ will be often used, which implies the coordinates $(\mathbf{r}_\perp, dj)$ in the a-b-c crystal frame. That is, x, y, and z axes are taken along the a, b, and c axes, respectively.

To describe a superconductor in a magnetic field tilted away from the a-b plane, we use a new rotated frame $(\tilde{x}-\tilde{y}-\tilde{z})$ defined by rotating the crystal frame $(x-y-z)$ around the x axis. It is expressed as

$$\tilde{x} = x, \quad \tilde{y} = y\cos\theta + z\sin\theta, \quad \tilde{z} = -y\sin\theta + z\cos\theta, \tag{3}$$

where the magnetic field is $\mathbf{H} = H(\hat{\mathbf{y}}\cos\theta + \hat{\mathbf{z}}\sin\theta) = H\hat{\tilde{\mathbf{y}}}$. Then, in the type-II limit with no spatial variation of the flux density, the vector potential is represented simply by

$$\mathbf{A}(\mathbf{r}) = (H\tilde{z},\ 0,\ 0) \tag{4}$$

in the $(\tilde{x},\ \tilde{y},\ \tilde{z})$ frame.

The second term of Eq. (1) represents an attractive interaction between quasiparticles, which leads to superconductivity, and, in the mean field approximation, may be expressed as

$$\mathcal{H}_{\rm SC} = \frac{1}{|g|}\sum_{\mathbf{q}}|\Delta(\mathbf{q})|^2 - \sum_{\mathbf{q}}\big(\Delta(\mathbf{q})\hat{\Psi}^\dagger(\mathbf{q}) + \text{H.c.}\big), \tag{5}$$

with

$$\hat{\Psi}(\mathbf{q}) = \frac{1}{2}\sum_{\mathbf{p},\alpha,\beta}(-i\hat{\sigma}_y)_{\alpha,\beta}\,w_{\mathbf{p}}\,\hat{c}_{-\mathbf{p}+\frac{\mathbf{q}}{2},\alpha}\hat{c}_{\mathbf{p}+\frac{\mathbf{q}}{2},\beta}, \qquad \Delta(\mathbf{q}) = |g|\langle\hat{\Psi}(\mathbf{q})\rangle. \tag{6}$$

Here, $\hat{\sigma}_i$ $(i = x,y,z)$ are the Pauli matrices. The SC pairing symmetry is represented by the pairing function $w_{\mathbf{p}}$, and, in the case of the $d_{x^2-y^2}$ pair, the identity $w_{\mathbf{p}+\mathbf{Q}_0} = -w_{\mathbf{p}}$ is satisfied, where $\mathbf{Q}_0 = (\pi/a,\pi/a,\pi/d)$ is the commensurate nesting vector represented with the lattice constant a in the a-b plane. After this identity has been used in the analytic treatment, $w_{\mathbf{p}}$ will be replaced by its linearized form $\sqrt{2}(\hat{p}_x^2 - \hat{p}_y^2)$ to perform the angle average over the Fermi surface.

The third term of Eq. (1) is the AFM interaction term and, in the mean field approximation, takes the form

$$\mathcal{H}_{\rm AFM} = \frac{1}{U}\sum_{\mathbf{q}}|\mathbf{m}(\mathbf{q})|^2 - \sum_{\mathbf{q}}(\mathbf{m}(\mathbf{q})\cdot\hat{\mathbf{S}}^\dagger(\mathbf{q}) + \text{H.c.}), \tag{7}$$

with

$$\hat{\mathbf{S}}(\mathbf{q}) = \sum_{\mathbf{p},\alpha,\beta} \hat{c}^{\dagger}_{\mathbf{p},\alpha} (\hat{\boldsymbol{\sigma}})_{\alpha,\beta} \hat{c}_{\mathbf{p}+\mathbf{Q}_0+\mathbf{q},\beta},$$
$$\mathbf{m}(\mathbf{q}) = U \langle \hat{\mathbf{S}}(\mathbf{q}) \rangle, \tag{8}$$

where the coupling constant U is assumed to be positive. Within the present model, an incommensurate nesting property will be incorporated in the dispersion relation in the manner

$$\xi(\mathbf{p}+\mathbf{Q}_0) = -\xi(\mathbf{p}) + \delta_{\mathrm{IC}} T_c, \tag{9}$$

where the deviation from a perfect nesting is represented by a constant parameter δ_{IC}. Then, we define the velocity $\mathbf{v}_{\mathbf{p}} = d\xi(\mathbf{p}_\perp)/d\mathbf{p}_\perp + J \sin(p_z d)\hat{z}$ and we have the relation

$$\mathbf{v}_{\mathbf{p}_\perp+\mathbf{Q}_0} = -\mathbf{v}_{\mathbf{p}_\perp}. \tag{10}$$

We note that the gap function $\Delta(\mathbf{q})$ and the staggered field $\mathbf{m}(\mathbf{q})$ play the roles of SC and AFM order parameters, respectively. Consistently with the previous theoretical works[7,9,13,14,34] and with the NMR data[8] in $CeCoIn_5$, we consider the case of a SC order parameter with a one-dimensional modulation of the Larkin-Ovchinnikov type[2] parallel to $\mathbf{H}$,

$$\Delta(\mathbf{r}) = |\Delta| \varphi_0(\tilde{z},\tilde{x}) \sqrt{2} \cos(q_{\mathrm{LO}} \tilde{y}), \tag{11}$$

as a reasonable model of the HFLT phase of $CeCoIn_5$. Here, the FFLO wave number q_{LO} plays the role of the order parameter representing the presence of a FFLO modulation and vanishes with the square-root field dependence $\sim \sqrt{H - H^*(T)}$ (see Sec. I) at the transition field H^* to the ordinary Abrikosov lattice state with $q_{\mathrm{LO}} = 0$. We note that, in $CeCoIn_5$ where the uniaxial anisotropy γ between the coherence lengths [see Eq. (13)] is moderate in magnitude,[35] it is reasonable to assume that the direction of the FFLO modulation is not deviated from $\mathbf{H}$ by tilting $\mathbf{H}$ from the a-b plane. The ordinary Abrikosov vortex lattice is expressed by the function φ_0 belonging to the lowest Landau level. In the present tilted field configuration, it takes the form

$$\varphi_0(\tilde{z},\tilde{x}) = \sqrt{\frac{k}{\sqrt{\pi}}} \sum_{n=-\infty}^{\infty} \exp\left[i\left(\frac{nk\Gamma(\theta)}{r_{\mathrm{H}}} \tilde{x} + \frac{\pi n^2}{2} \right) - \frac{1}{2}\left(\frac{1}{r_{\mathrm{H}}\Gamma(\theta)} \tilde{z} + nk \right)^2 \right] \tag{12}$$

with integer n, where $r_{\mathrm{H}} = 1/\sqrt{2eH}$, and the angle-dependent factor $\Gamma(\theta)$ is associated with the material anisotropy and described as

$$\Gamma^4(\theta) = \sin^2\theta + \frac{1}{\gamma^2}\cos^2\theta,$$
$$\gamma = \sqrt{\frac{\langle v_x^2 \rangle_{\mathrm{FS}}}{\langle v_z^2 \rangle_{\mathrm{FS}}}} = \frac{2\sqrt{1 - J/\mu}}{\pi J/\mu}. \tag{13}$$

As shown in our previous works,[13,14] the FFLO modulation of the SC order parameter should induce a spatial modulation parallel to $\mathbf{H}$ of the AFM order parameter through a coupling term $f^{(2,2)}_{\Delta,m}$ [see Eqs. (16) and (32)] in the free energy with the SC order parameter. Naively, we choose the form

$$\mathbf{m}(\mathbf{r}) = \sum_{\mathbf{q}} |\mathbf{m}| e^{i\mathbf{q}\cdot\mathbf{r}} \sqrt{2} \cos(q_{\mathrm{LO}} \tilde{y} + \phi) \tag{14}$$

for the AFM order parameter. For simplicity, we focus on the situation in which the FFLO modulation wave number q_{LO} is much smaller than that of the AFM modulation, so that *nonlocal* couplings, proportional to q^2_{LO}, between the AFM and FFLO orders may be negligible. That is, through the last factor $\cos(q_{\mathrm{LO}}\tilde{y} + \phi)$ in Eq. (14), just the local coupling between the spatial modulations parallel to the magnetic field of the two order parameters will be taken into account.[14] Hereafter, this treatment will be called as the *local approximation*.

As illustrated in Fig. 1, in the case of $\phi = 0$, the AFM order primarily appears in the region where $|\Delta|$ is maximal, while it appears, when $\phi = \pi/2$, primarily in the vicinity of the FFLO nodal plane on which $\Delta = 0$. Hereafter, we call the former as the *in-phase* configuration and the latter as the *out-of-phase* one. Strictly speaking, the transformation between the two structures indicated in Fig. 1 seems to occur through two continuous transitions (see Ref. 46 of Ref. 14). Nevertheless, for simplicity, we restrict ourselves to these two structures throughout this paper. Further, we assume the direction $\mathbf{m}$ of the AFM moment to be locked along the z axis corresponding to the c axis of the Q2D material (see the caption of Fig. 2 and Sec. I). In this case, we have $\mathbf{m}(\mathbf{r}) = m(\mathbf{r})\hat{\mathbf{z}} = m(\mathbf{r})(\hat{\tilde{\mathbf{y}}} \sin\theta + \hat{\tilde{\mathbf{z}}} \cos\theta)$.

A. Ginzburg-Landau free energy

The mean field free-energy density for the Hamiltonian defined above is given by

$$f_{\mathrm{GL}}(\Delta, m, q_{\mathrm{LO}}) = -V^{-1} T \ln \mathrm{Tr}_{c,c^\dagger} \times \{\exp[-(\mathcal{H}_0 + \mathcal{H}_{\mathrm{SC}} + \mathcal{H}_{\mathrm{AFM}})/T]\}. \tag{15}$$

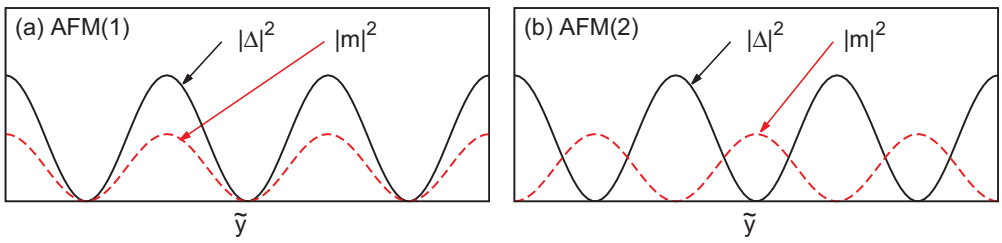

FIG. 1. (Color online) Typical configurations in real space of the AFM order [dashed (red) curve] in the FFLO state with one-dimensional spatial modulation of the amplitude $|\Delta|$ of the SC order parameter [solid (black) curve] parallel to the field. In the in-phase structure (a), the AFM order favors coexistence with the SC order, while, in the out-of-phase structure (b), it tends to lie around the nodal planes, on which $|\Delta| = 0$, of the FFLO modulation (see the text). These states correspond to the $\phi = 0$ and $\pi/2$ cases in Eq. (14), respectively.

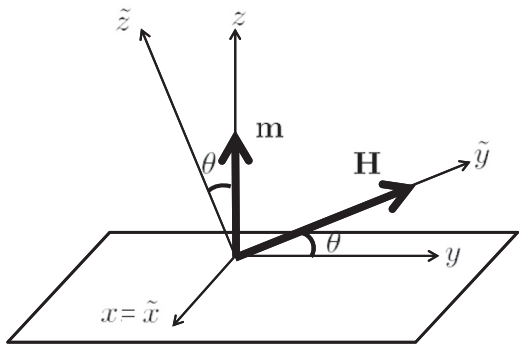

FIG. 2. Coordinate frames used in the present calculations. The x-y-z frame corresponds to the crystal a, b, and c frames of a uniaxial crystal and the frame $\tilde{x}$-$\tilde{y}$-$\tilde{z}$ with the magnetic field $\mathbf{H}$ in the $\tilde{\mathbf{y}}$ direction is obtained by the θ rotation of the x-y-z frame about the x axis. According to Ref. 27 on $CeCoIn_5$, the orientation of the moment $\mathbf{m}$ is assumed to be locked in the c direction irrespective of the $\mathbf{H}$ direction.

In the present situation including the AFM and FFLO orders, we consider the following Ginzburg-Landau (GL) form of the free-energy density expressed in powers of the order parameters $|\Delta|$ and $m \equiv |\mathbf{m}|$:

$$f_{\rm GL}(\Delta,m,q_{\rm LO}) = f_\Delta^{(2)}(q_{\rm LO}) + f_\Delta^{(4)}(q_{\rm LO}) + f_\Delta^{(6)} + f_m^{(2)} + f_m^{(4)} + f_{\Delta m}^{(2,2)}, \tag{16}$$

where

$$f_\Delta^{(2)}(q_{\rm LO}) = f_\Delta^{(2,0)} + f_\Delta^{(2,2)} q_{\rm LO}^2 + f_\Delta^{(2,4)} q_{\rm LO}^4,$$
$$f_\Delta^{(4)}(q_{\rm LO}) = f_\Delta^{(4,0)} + f_\Delta^{(4,2)} q_{\rm LO}^2 + f_\Delta^{(4,4)} q_{\rm LO}^4. \tag{17}$$

Since the present AFM ordering is enhanced or induced by the SC ordering, we can assume that the SC order is rigid enough and thus is unaffected by the AFM ordering, especially if the high-field H_{c2} transition is discontinuous as a consequence of the strong PPB.[4] That is, we determine the SC energy gap by focusing on the m-independent terms. In our GL approach taking account of the orbital pair breaking, other higher-order terms in Δ have been neglected.[14,32] We have repeatedly checked that, in low temperatures and high fields of our interest, the conditions $f_\Delta^{(4)} < 0$ and $f_\Delta^{(6)} > 0$ are always satisfied so that the H_{c2} transition is discontinuous, while truncating the GL expansion in the sixth order in $|\Delta|$ is permitted. On the other hand, the FFLO transition line, i.e., the onset of the FFLO modulation of the SC order parameter, is determined through the appearance of a nonvanishing $q_{\rm LO}$ according to the expressions (17).

Here, we should mention that the local approximation has been taken, as in Ref. 14, in other free-energy terms including the AFM order parameter m such as the coupling term $f_{\Delta m}^{(2,2)}$ of the AFM and SC orders [see also the sentence following Eq. (14)]. We note that the sign of $f_{\Delta m}^{(2,2)}$, proportional to $|\Delta|^2$, is negative in systems with strong enough PPB and in the range of the tilt angle where the AFM order is realized at finite temperatures. This sign favors the in-phase structure illustrated in Fig. 1(a) of the AFM order in real space. However, it will be shown in Sec. III that this result may be an artifact of the use of the GL expansion in Δ.

B. GL coefficients

Now, we turn to the calculation of the coefficient of each term in the GL free-energy density. To obtain each GL coefficient, we apply the semiclassical approximation

$$\mathcal{G}_{\varepsilon_n,\sigma}^{(H)}(\mathbf{r},\mathbf{r}') \simeq \mathcal{G}_{\varepsilon_n,\sigma}(\mathbf{r}-\mathbf{r}') \exp\left(ie\int_{\mathbf{r}}^{\mathbf{r}'} d\mathbf{s}\cdot\mathbf{A}(\mathbf{s})\right) \tag{18}$$

for the normal Green's function $\mathcal{G}_{\varepsilon_n,\sigma}^{(H)}$ in a magnetic field, where $\mathcal{G}_{\varepsilon_n,\sigma}(\mathbf{r}-\mathbf{r}')$ appearing in the right-hand side is the Green's function in the case with no orbital pair breaking of the magnetic field, and its Fourier transformation is expressed by

$$\mathcal{G}_{\varepsilon_n,\sigma}(\mathbf{p}) = \{i\varepsilon_n - \xi(\mathbf{p}_\perp) + J[1-\cos(p_z d)] + \sigma I\}^{-1}, \tag{19}$$

where $\varepsilon_n = (2n+1)\pi T$ is the fermion's Matsubara frequency. Further, the orbital pair-breaking effect is incorporated by the gradient $\Pi = -i\nabla + 2e\mathbf{A}(\mathbf{r})$ operating on the pair fields through the formula

$$\exp\left(2ie\int_{\mathbf{r}}^{\mathbf{r}'} d\mathbf{s}\cdot\mathbf{A}(\mathbf{s})\right)\Delta(\mathbf{r}') = \exp\left[-i(\mathbf{r}-\mathbf{r}')\cdot\Pi\right]\Delta(\mathbf{r}). \tag{20}$$

Then, the quadratic, quartic, and sixth-order terms in Δ of the GL free-energy density are represented by

$$f_\Delta^{(2)}(q_{\rm LO}) = \left\langle \Delta^*(\mathbf{r})\left[\frac{1}{|g|} - K_\Delta^{(2)}(\Pi)\right]\Delta(\mathbf{r})\right\rangle_{\rm sp},$$
$$K_\Delta^{(2)} = \frac{T}{2}\sum_{\varepsilon_n,\mathbf{p},\sigma} |w_\mathbf{p}|^2 \mathcal{G}_{\varepsilon_n,\sigma}(\mathbf{p})\mathcal{G}_{-\varepsilon_n,-\sigma}(-\mathbf{p}+\Pi),$$
$$f_\Delta^{(4)}(q_{\rm LO}) = \left\langle K_\Delta^{(4)}(\Pi_i)\Delta^*(\mathbf{s}_1)\Delta(\mathbf{s}_2)\Delta^*(\mathbf{s}_3)\Delta(\mathbf{s}_4)\big|_{\mathbf{s}_i\to\mathbf{r}}\right\rangle_{\rm sp},$$
$$K_\Delta^{(4)} = \frac{T}{4}\sum_{\varepsilon_n,\mathbf{p},\sigma} |w_\mathbf{p}|^4 \mathcal{G}_{\varepsilon_n,\sigma}(\mathbf{p})\mathcal{G}_{-\varepsilon_n,-\sigma}(-\mathbf{p}+\Pi_1^\dagger) \times \mathcal{G}_{-\varepsilon_n,-\sigma}(-\mathbf{p}+\Pi_2)\mathcal{G}_{\varepsilon_n,\sigma}(\mathbf{p}+\Pi_3^\dagger-\Pi_2),$$
$$f_\Delta^{(6)}(q_{\rm LO}) = \left\langle K_\Delta^{(6)}(\Pi_i)\Delta^*(\mathbf{s}_1)\Delta(\mathbf{s}_2)\Delta^*(\mathbf{s}_3)\Delta(\mathbf{s}_4) \times \Delta^*(\mathbf{s}_5)\Delta(\mathbf{s}_6)\big|_{\mathbf{s}_i\to\mathbf{r}}\right\rangle_{\rm sp},$$
$$K_\Delta^{(6)} = \frac{T}{6}\sum_{\varepsilon_n,\mathbf{p},\sigma} |w_\mathbf{p}|^6 \mathcal{G}_{\varepsilon_n,\sigma}(\mathbf{p})\mathcal{G}_{-\varepsilon_n,-\sigma}(-\mathbf{p}+\Pi_1^\dagger) \times \mathcal{G}_{-\varepsilon_n,-\sigma}(-\mathbf{p}+\Pi_6)\mathcal{G}_{\varepsilon_n,\sigma}(\mathbf{p}-\Pi_1^\dagger-\Pi_2) \times \mathcal{G}_{-\varepsilon_n,-\sigma}(-\mathbf{p}+\Pi_1^\dagger+\Pi_3^\dagger-\Pi_2) \times \mathcal{G}_{\varepsilon_n,\sigma}(\mathbf{p}-\Pi_6+\Pi_5^\dagger). \tag{21}$$

The concrete expressions of these terms are represented in the Appendix. In obtaining them, we need to rewrite the expression $\exp(iA\mathbf{v}_\mathbf{p}\cdot\Pi)\Delta(\mathbf{r})$. To perform this, it will be represented in the rotated frame as follows:

$$\exp(iA\mathbf{v}_\mathbf{p}\cdot\Pi) = \exp(iA\tilde{\boldsymbol{v}}_{\tilde{p}}\cdot\tilde{\boldsymbol{\Pi}}) = \exp(iA\tilde{v}_{\tilde{p},\tilde{y}}\tilde{\Pi}_{\tilde{y}})\exp(iA\tilde{\boldsymbol{v}}_{\tilde{p},\perp}\cdot\tilde{\boldsymbol{\Pi}}_\perp), \tag{22}$$

where $\tilde{\boldsymbol{v}}_{\tilde{p},\perp} = (\tilde{v}_{\tilde{p},\tilde{z}}, \tilde{v}_{\tilde{p},\tilde{x}})$ and $\tilde{\boldsymbol{\Pi}}_\perp = (\tilde{\Pi}_{\tilde{z}}, \tilde{\Pi}_{\tilde{x}})$ represent the components perpendicular to the field ($\parallel \tilde{y}$ axis) of $\mathbf{v_p}$ and Π in the rotated frame (see Fig. 2). By introducing the creation and annihilation operators on the Landau levels representing possible vortex states

$$\tilde{\Pi}_\pm = \frac{r_{\rm H}}{\sqrt{2}}[\Gamma(\theta)\tilde{\Pi}_{\tilde{z}} \pm i\Gamma^{-1}(\theta)\tilde{\Pi}_{\tilde{x}}], \tag{23}$$

we find

$$\exp(iA\tilde{\boldsymbol{v}}_{\tilde{p},\perp}\cdot\tilde{\boldsymbol{\Pi}}_\perp) = \exp\left(-\tfrac{1}{2}|\mu|^2A^2\right)\exp(i\mu\tilde{\Pi}_+A) \times \exp(i\mu^*\tilde{\Pi}_-A), \tag{24}$$

where

$$\mu = \frac{\Gamma^{-1}(\theta)\tilde{v}_{\tilde{p},\tilde{z}} - i\Gamma(\theta)\tilde{v}_{\tilde{p},\tilde{x}}}{\sqrt{2}r_{\rm H}T_c}. \tag{25}$$

Next, we calculate the GL terms associated with the AFM order parameter $\mathbf{m}$. The expression of the term quadratic in $\mathbf{m}$ is given by

$$f_m^{(2)} = \left\langle\left[\frac{1}{U} + \sum_{j=1}^{2} K_{m,j}^{(2)}(\mathbf{q})\right]|m(\mathbf{r})|^2\right\rangle_{\rm sp}, \tag{26}$$

where $\mathbf{q}$ is the incommensurate part of the AFM wave vector which should be determined by minimizing the free energy, and the concrete expression of $K_{m,j}^{(2)}$ is

$$\begin{aligned} K_{m,j}^{(2)}(\mathbf{q}) &= \frac{A_jT}{2}\sum_{\varepsilon_n,\mathbf{p},\sigma}\mathcal{G}_{\varepsilon_n,\sigma}(\mathbf{p})\mathcal{G}_{\varepsilon_n,\alpha_j}(\mathbf{p}+\mathbf{Q}_0+\mathbf{q}) \\ &= -A_j\pi TN(0) \\ &\quad\times\sum_{\varepsilon_n,\sigma}\left\langle\frac{is_\epsilon}{2i\varepsilon_n + (\sigma+\alpha_j)I - \delta_{\rm IC}T_c + \mathbf{v_p}\cdot\mathbf{q}}\right\rangle_{\rm FS} \\ &= -A_jN(0)\int_0^\infty d\rho\, f(\rho,B_j) \\ &\quad\times\left\langle\cos\left[\left(-\delta_{\rm IC}+\frac{\mathbf{v_p}\cdot\mathbf{q}}{T_c}\right)\rho\right]\right\rangle_{\rm FS}. \end{aligned} \tag{27}$$

TABLE I. Coefficients α_j, A_j, B_j in Eqs. (27) and (31).

j	α_j	A_j	B_j
1	$-\sigma$	$\cos^2\theta$	0
2	σ	$\sin^2\theta$	ρ

Here, the angle brackets denote the Fermi surface average, $N(0)$ is the density of states at the Fermi energy, s_ϵ is the sign of ε_n,

$$f(x,y) = \frac{2\pi t}{\sinh(2\pi tx)}\cos\left(2\frac{I}{T_c}y\right), \tag{28}$$

with $t = T/T_c$, and the coefficients α_j, A_j, B_j are represented in Table I. Here, the identity

$$\frac{1}{\alpha} = \int_0^\infty d\rho\,\exp(-\alpha\rho)\ ({\rm Re}\,\alpha > 0) \tag{29}$$

was used in obtaining Eq. (27).

By using Eq. (29), the coupling constant U is represented by

$$\begin{aligned} \frac{1}{U} &= N(0)\left(\ln\frac{T}{T_{\rm N}} + 2\pi T\sum_{\varepsilon_n>0}\frac{1}{\varepsilon_n}\right) \\ &= N(0)\left(\ln\frac{T}{T_{\rm N}} + \int_0^\infty d\rho\, f(\rho,0)\right), \end{aligned} \tag{30}$$

where $T_{\rm N}$ is the AFM transition temperature in the normal state. Then, the quadratic term in $\mathbf{m}$ is expressed by

$$f_m^{(2)} = N(0)T_c^2\left[\ln\frac{T}{T_{\rm N}} + \int_0^\infty d\rho\left(f(\rho,0) - \sum_{j=1}^{2}A_jf(\rho,B_j)\left\langle\cos\left[\left(-\delta_{\rm IC}+\frac{\mathbf{v_p}\cdot\mathbf{q}}{T_c}\right)\rho\right]\right\rangle_{\rm FS}\right)\right]\left(\frac{|m|}{T_c}\right)^2. \tag{31}$$

Further, the term giving the coupling between the SC and magnetic orders is expressed by

$$f_{\Delta m}^{(2,2)} = \left\langle\left[\sum_{j=1}^{4}K_{\Delta m,j}^{(2,2)}(\Pi_s,\mathbf{q})\right]\Delta^*(\mathbf{r})\Delta(\mathbf{s})\Big|_{\mathbf{s}\to\mathbf{r}}|m(\mathbf{r})|^2\right\rangle_{\rm sp}, \tag{32}$$

where the kernels $K^{(2,2)}$ with $j = 1,2$ take the form

$$\begin{aligned} K_{\Delta m,j}^{(2,2)}(\Pi_s,\mathbf{q}) &= \frac{A_j'T}{2}\sum_{\varepsilon_n,\mathbf{p},\sigma}|w_\mathbf{p}|^2\mathcal{G}_{\varepsilon_n,\sigma}(\mathbf{p})\mathcal{G}_{\varepsilon_n,\alpha_j'}(\mathbf{p}-\mathbf{Q}_0-\mathbf{q})\mathcal{G}_{\varepsilon_n,\sigma}(\mathbf{p})\mathcal{G}_{-\varepsilon_n,-\sigma}(-\mathbf{p}+\Pi_\mathbf{s}) \\ &= A_j'\pi TN(0)\sum_{\varepsilon_n>0,\sigma,s_\epsilon}\left\langle|w_\mathbf{p}|^2\frac{is_\epsilon}{[2i\varepsilon_n+(\sigma+\alpha_j')I-\delta_{\rm IC}T_c-\mathbf{v_p}\cdot\mathbf{q}](2i\varepsilon_n+2\sigma I-\mathbf{v_p}\cdot\Pi_\mathbf{s})}\right. \\ &\quad\times\left.\left(\frac{1}{2i\varepsilon_n+(\sigma+\alpha_j')I-\delta_{\rm IC}T_c-\mathbf{v_p}\cdot\mathbf{q}} - \frac{1}{2i\varepsilon_n+2\sigma I-\mathbf{v_p}\cdot\Pi_\mathbf{s}}\right)\right\rangle_{\rm FS} \end{aligned}$$

$$= \frac{A'_j N(0)}{2} \sum_{s_\epsilon} \int_0^\infty \prod_{i=1}^{3} d\rho_i \left[f\left(\sum_{i=1}^{3} \rho_i, B'_j\right) \left\langle |w_{\mathbf{p}}|^2 \exp\left[-is_\epsilon \left(-\delta_{\rm IC} + \frac{\mathbf{v_p}\cdot\mathbf{q}}{T_c}\right) C'_j \right] \exp\left(-is_\epsilon \mathbf{v_p}\cdot\Pi_{\mathbf{s}} D'_j\right) \right\rangle_{\rm FS} \right.$$
$$\left. + f\left(\sum_{i=1}^{3} \rho_i, E'_j\right) \left\langle |w_{\mathbf{p}}|^2 \exp\left[-is_\epsilon \left(-\delta_{\rm IC} + \frac{\mathbf{v_p}\cdot\mathbf{q}}{T_c}\right) F'_j \right] \exp\left(-is_\epsilon \frac{\mathbf{v_p}\cdot\Pi_{\mathbf{s}}}{T_c} G'_j\right) \right\rangle_{\rm FS} \right], \tag{33}$$

while, for $j = 3,4$, these kernels are expressed, in terms of the property $w_{\mathbf{p}+\mathbf{Q}_0} = -w_{\mathbf{p}}$ on the $d_{x^2-y^2}$-wave pairing function, by

$$K^{(2,2)}_{\Delta m,\, j}(\Pi_s, \mathbf{q}) = -\frac{A'_j T}{2} \sum_{\varepsilon_n, \mathbf{p}, \sigma} w_{\mathbf{p}} w_{\mathbf{p}+\mathbf{Q}_0} \mathcal{G}_{\varepsilon_n,\sigma}(\mathbf{p}) \mathcal{G}_{\varepsilon_n,\alpha'_j}(\mathbf{p}-\mathbf{Q}_0-\mathbf{q}) \mathcal{G}_{-\varepsilon_n,\alpha'_j}(-\mathbf{p}+\mathbf{Q}_0+\mathbf{q}+\Pi_{\mathbf{s}}) \mathcal{G}_{-\varepsilon_n,-\sigma}(-\mathbf{p}+\Pi_{\mathbf{s}})$$
$$= -A'_j \pi T N(0) \sum_{\varepsilon_n>0,\sigma,s_\epsilon} \left\langle |w_{\mathbf{p}}|^2 \frac{is_\epsilon}{[2i\varepsilon_n + (\sigma+\alpha'_j)I - \delta_{\rm IC} T_c - \mathbf{v_p}\cdot\mathbf{q}]} \right.$$
$$\left. \times \frac{1}{[2i\varepsilon_n + (\sigma+\alpha'_j)I + \delta_{\rm IC} T_c + \mathbf{v_p}\cdot\mathbf{q}]} \left(\frac{1}{2i\varepsilon_n + 2\sigma I - \mathbf{v_p}\cdot\Pi_{\mathbf{s}}} - \frac{1}{2i\varepsilon_n + 2\alpha'_j I + \mathbf{v_p}\cdot\Pi_{\mathbf{s}}} \right) \right\rangle_{\rm FS}$$
$$= \frac{A'_j N(0)}{2} \sum_{s_\epsilon} \int_0^\infty \prod_{i=1}^{3} d\rho_i \left[f\left(\sum_{i=1}^{3} \rho_i, B'_j\right) \left\langle |w_{\mathbf{p}}|^2 \exp\left[-is_\epsilon \left(-\delta_{\rm IC} + \frac{\mathbf{v_p}\cdot\mathbf{q}}{T_c}\right) C'_j \right] \exp\left(-is_\epsilon \frac{\mathbf{v_p}\cdot\Pi_{\mathbf{s}}}{T_c} D'_j\right) \right\rangle_{\rm FS} \right.$$
$$\left. + f\left(\sum_{i=1}^{3} \rho_i, E'_j\right) \left\langle |w_{\mathbf{p}}|^2 \exp\left[-is_\epsilon \left(-\delta_{\rm IC} + \frac{\mathbf{v_p}\cdot\mathbf{q}}{T_c}\right) F'_j \right] \exp\left(-is_\epsilon \frac{\mathbf{v_p}\cdot\Pi_{\mathbf{s}}}{T_c} G'_j\right) \right\rangle_{\rm FS} \right]. \tag{34}$$

The coefficients α'_j, A'_j, B'_j, C'_j, D'_j, E'_j, F'_j, G'_j are represented in Table II.

By using the above-mentioned mathematical tools, we obtain

$$f^{(2,2)}_{\Delta m} = \frac{3N(0)T_c^2}{2} \sum_{j=1}^{4} A'_j \int_0^\infty \prod_{i=1}^{3} d\rho_i \left[f\left(\sum_{i=1}^{3} \rho_i, B'_j\right) \left\langle |w_{\mathbf{p}}|^2 \cos\left[\left(-\delta_{\rm IC} + \frac{\mathbf{v_p}\cdot\mathbf{q}}{T_c}\right) C'_j \right] \exp\left(-\frac{|\mu|^2}{2} D'_j\right) \right\rangle_{\rm FS} \right.$$
$$\left. + f\left(\sum_{i=1}^{3} \rho_i, E'_j\right) \left\langle |w_{\mathbf{p}}|^2 \cos\left[\left(-\delta_{\rm IC} + \frac{\mathbf{v_p}\cdot\mathbf{q}}{T_c}\right) F'_j \right] \exp\left(-\frac{|\mu|^2}{2} G'_j\right) \right\rangle_{\rm FS} \right] \left(\frac{|\Delta|}{T_c}\right)^2 \left(\frac{|m|}{T_c}\right)^2. \tag{35}$$

Finally, the quartic term $f^{(4)}_m$ in $\mathbf{m}$ is expressed as

$$f^{(4)}_m = \left\langle \left[\sum_{j=1}^{5} K^{(4)}_{m,\, j}(\mathbf{q}) \right] |m(\mathbf{r})|^4 \right\rangle_{\rm sp}, \tag{36}$$

where

$$K^{(4)}_{m,\, j}(\mathbf{q}) = \frac{A''_j T}{2} \sum_{\varepsilon_n, \mathbf{p}, \sigma} \mathcal{G}_{\varepsilon_n,\sigma}(\mathbf{p}) \mathcal{G}_{\varepsilon_n,\alpha''_j}(\mathbf{p}+\mathbf{Q}_0+\mathbf{q}) \mathcal{G}_{\varepsilon_n,\beta''_j}(\mathbf{p}) \mathcal{G}_{\varepsilon_n,\gamma''_j}(\mathbf{p}+\mathbf{Q}_0+\mathbf{q})$$
$$= N(0) A''_j \int_0^\infty \prod_{i=1}^{3} d\rho_i \left[f\left(\sum_{i=1}^{3} \rho_i, B''_j\right) + f\left(\sum_{i=1}^{3} \rho_i, C''_j\right) \right] \left\langle \cos\left[\left(-\delta_{\rm IC} + \frac{\mathbf{v_p}\cdot\mathbf{q}}{T_c}\right) \left(\sum_{i=1}^{3} \rho_i\right) \right] \right\rangle_{\rm FS}. \tag{37}$$

Then, the corresponding term in the free energy is expressed as

$$f^{(4)}_m = \frac{3N(0)T_c^2}{2} \sum_{j=1}^{5} A''_j \int_0^\infty \prod_{i=1}^{3} d\rho_i \left[f\left(\sum_{i=1}^{3} \rho_i, B''_j\right) + f\left(\sum_{i=1}^{3} \rho_i, C''_j\right) \right] \left\langle \cos\left[\left(-\delta_{\rm IC} + \frac{\mathbf{v_p}\cdot\mathbf{q}}{T_c}\right) \left(\sum_{i=1}^{3} \rho_i\right) \right] \right\rangle_{\rm FS} \left(\frac{|m|}{T_c}\right)^4. \tag{38}$$

The coefficients α''_j, β''_j, γ''_j, A''_j, B''_j, C''_j are listed in Table III. The resulting numerical calculation results are characterized by the Maki parameter

$$\alpha_{\rm M}(\theta) = \frac{\sqrt{2} H^\theta_{\rm orb}(0)}{H^\theta_{\rm P}(0)} \tag{39}$$

generalized to the case with the tilt angle θ, which measures the relative strength of the paramagnetic and orbital pair-breaking effects at the angle θ. Here, $H^\theta_{\rm P}(0)$ is the Pauli-limiting field at $T = 0$ and at the angle θ and is defined as $\pi T_c/[2e^{\gamma_{\rm E}}\mu_{\rm B} g(\theta)]$, where $e^{\gamma_{\rm E}} = 1.77$ is the Euler constant, while the $T = 0$ orbital-limiting field $H^\theta_{\rm orb}(0)$

TABLE II. Coefficients α'_j, A'_j, B'_j, C'_j, D'_j, E'_j, F'_j, G'_j in Eqs. (33), (34), and (35).

j	α'_j	A'_j	B'_j	C'_j	D'_j	E'_j	F'_j	G'_j
1	$-\sigma$	$2\cos^2\theta$	ρ_2	$\rho_1+\rho_3$	ρ_2	$\rho_2+\rho_3$	ρ_1	$\rho_2+\rho_3$
2	σ	$2\sin^2\theta$	ρ_2	$\rho_1+\rho_3$	ρ_2	$\rho_2+\rho_3$	ρ_1	$\rho_2+\rho_3$
3	$-\sigma$	$\cos^2\theta$	ρ_3	$-\rho_1+\rho_2$	ρ_3	ρ_3	$-\rho_1+\rho_2$	$-\rho_3$
4	σ	$\sin^2\theta$	$\sum_{i=1}^3\rho_i$	$-\rho_1+\rho_2$	ρ_3	$\sum_{i=1}^3\rho_i$	$-\rho_1+\rho_2$	$-\rho_3$

satisfies $H^{\theta}_{\rm orb}(0)=H^{(\theta=0)}_{\rm orb}(0)/\gamma\Gamma^2(\theta)$. Both of these two limiting fields decrease with tilting the field direction from the a-b plane. In our numerical calculations, we use the parameter values $g_c/g_a=2.1$, $\gamma=2.8$, and $\alpha_{\rm M}(0)=6.11$.

C. Results

Figure 3 shows possible H versus T phase diagrams for tilt angles $\theta=0^\circ$, 18°, 22°, and 30°, respectively. The dotted (red) lines express the second-order transition between the ordinary vortex state and the FFLO vortex lattice, and, in the low-temperature region shown here, the mean field SC transition on $H_{c2}(T)$, expressed by the black solid curve, is of first order in character in the mean field approximation.[4] On the other hand, the character of the AFM ordering transition in the SC phase, occurring on the dashed (blue) curve, seems to depend on the parameters such as the tilt angle θ, although it tends to become of second order in most situations. Its detail will be discussed at the end of Sec. III.

As one can see in Fig. 3(a) where $\theta=0^\circ$, the AFM order appears only in the FFLO region. As indicated in Refs. 13 and 14, the AFM ordering is enhanced by the FFLO order and stabilized with a spatial modulation commensurate with that of the FFLO state. Such appearance of the AFM order is consistent with that found in experiments on $CeCoIn_5$.[8,11,12] On the other hand, contrary to the experimental fact,[8,11,12] a *nonmagnetic* FFLO region with no accompanying AFM order inevitably appears at higher temperatures in our calculation shown in Fig. 3. However, if AFM fluctuation effects are incorporated beyond the present mean field treatment, this FFLO region is expected to shrink significantly.[9]

Regarding the relative spatial structure in the direction parallel to the field between the AFM and FFLO orders, just the in-phase configuration expressed in Fig. 1(a) and denoted as FFLO + AFM(1) in Fig. 3 is found to be realized even in $\theta\neq0^\circ$ cases in the present approach using the GL expansion in Δ. This feature, inconsistent with the experimental data,[30] is found in the next section to be an artifact of the present GL approach keeping only the lowest term proportional to $|\Delta|^2\,m^2$ regarding the coupling between the AFM and SC orders (see also Ref. 14).

Next, the angular dependencies of the resulting two orders will be discussed. As the field is tilted away from the conducting plane in the uniaxial material, the relative contribution of the orbital pair breaking increases, while effects of PPB diminish. Since both of the FFLO and AFM orders have their origin in PPB for the d-wave SC pairing state, the field tilt implies that both of the orders are suppressed at higher angles. However, the AFM order has another origin on its suppression due to the field tilt: The Zeeman effect on the AFM ordering occurring from the field component parallel to the AFM moment **m** becomes an origin of its suppression: As seen in the difference between $j=1$ and 2 components in Eq. (31), the nesting property gradually becomes unsatisfactory with increasing the tilt angle. Consequently, the AFM order diminishes more remarkably than the FFLO order with tilting the field, and a tilt instability of the AFM order should occur at a lower angle than a threshold angle at which the FFLO phase is lost. Then, a nonmagnetic FFLO phase with no accompanying AFM order needs to exist at lower angles than the FFLO threshold angle. This picture suggested by Fig. 3 is consistent with the experimental fact.[27–29]

Further, when the field value H increases, the above-mentioned reduction of the nesting condition due to an increase of the field component parallel to **m** competes with the enhancement of the AFM order due to stronger PPB in larger H. Due to this competition, the magnetic field values at which the AFM order is realized at finite temperatures should lie at a lower field than $H_{c2}(T=0)$. This explains why the dashed (blue) curve in Fig. 3(b) shows a field-induced disappearance of the AFM order in contrast to that in Fig. 3(a). This result implies that the AFM quantum critical point (QCP), which should occur at an angle between 18° and 22° in the case of Fig. 3, should also lie at a lower field than $H_{c2}(0)$.

TABLE III. Coefficients α''_j, β''_j, γ''_j, A''_j, B''_j, C''_j in Eqs. (37) and (38).

j	α''_j	β''_j	γ''_j	A''_j	B''_j	C''_j
1	$-\sigma$	σ	$-\sigma$	$\cos^4\theta$	0	0
2	σ	σ	σ	$\sin^4\theta$	$\sum_{i=1}^3\rho_i$	$\sum_{i=1}^3\rho_i$
3	σ	σ	$-\sigma$	$2\cos^2\theta\sin^2\theta$	ρ_1	$\rho_1+\rho_3$
4	σ	$-\sigma$	σ	$2\cos^2\theta\sin^2\theta$	$\rho_1+\rho_3$	ρ_1
5	σ	$-\sigma$	$-\sigma$	$-2\cos^2\theta\sin^2\theta$	$\rho_1-\rho_2$	$\rho_1-\rho_2$

III. PAULI LIMIT

In turn, following the previous work,[14] we will explain our results in the Pauli limit performed in order to examine consequences of the band structure on the HFLT phase of $CeCoIn_5$. For this purpose, we start from the conventional tight-binding Hamiltonian with a dispersion $\varepsilon(\mathbf{p})$. Broadly, the basic elements in the Hamiltonian are the same as those in the previous section. The only differences are to replace $\mathcal{H}_{kin}$ in the previous section by

$$\mathcal{H}'_0=\sum_\sigma\int d^3\mathbf{r}[\psi^{(\sigma)}]^\dagger(\mathbf{r})[\varepsilon(-i\nabla)-\sigma I]\psi^{(\sigma)}(\mathbf{r}) \qquad (40)$$

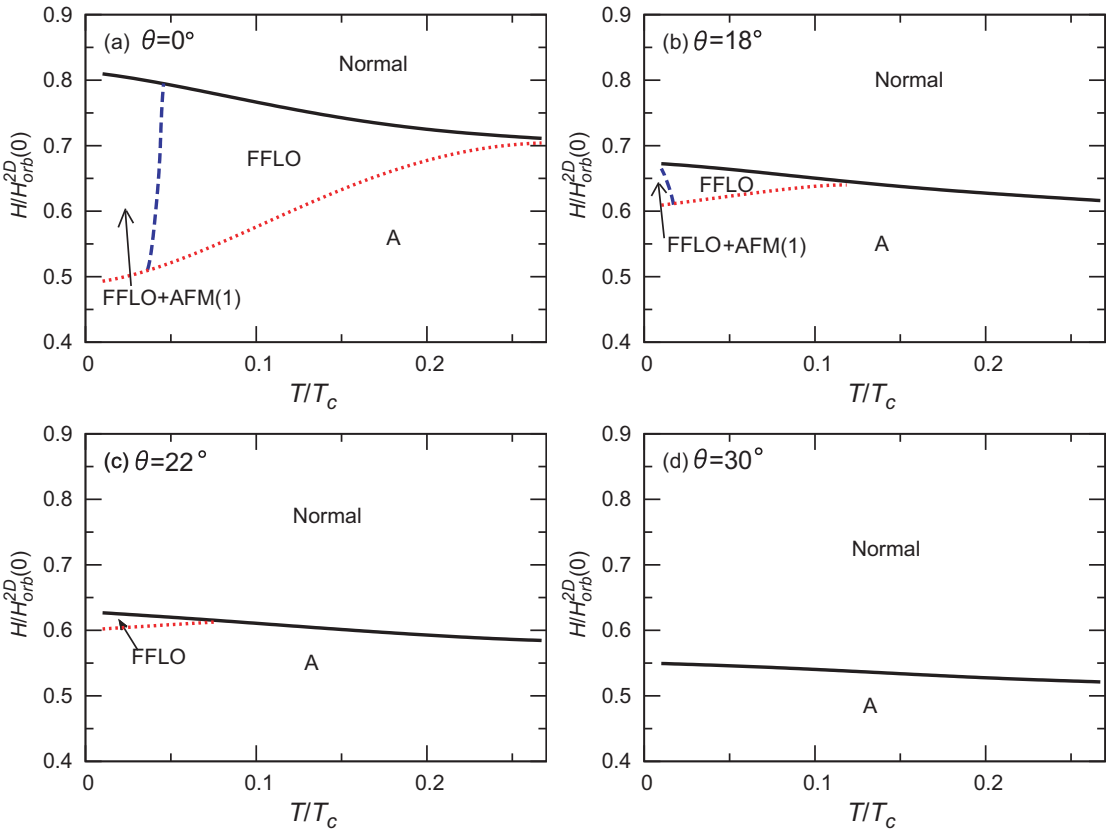

FIG. 3. (Color online) Angular dependence of the H-T phase diagrams for the $\theta = 0^\circ$, 18°, 22°, and 30° cases. The dotted (red) and the thick solid (black) lines express the curves of the second-order transition curve from the Abrikosov lattice (A) phase to the FFLO one and of the discontinuous $H_{c2}(T)$ transition, respectively, while the dashed (blue) line represents the nonmagnetic FFLO to the AFM-FFLO transition. In this calculation, the parameters $\alpha_{\rm M}(0) = 6.11$, the incommensurability $\delta = 0.001$, $\gamma = 2.8$, $g_c/g_a = 2.1$, and $T_{\rm N}/T_{\rm c} = 0.0012$ are used.

with

$$\psi^{(\sigma)}(\mathbf{r}) = \frac{1}{\sqrt{V}}\sum_{\mathbf{p}} \hat{c}_{\mathbf{p},\sigma} e^{i\mathbf{p}\cdot\mathbf{r}},$$
$$\begin{aligned}\varepsilon(\mathbf{p}) = &-2t_1[\cos(p_x a) + \cos(p_y a)] \\ &- 4t_2\cos(p_x a)\cos(p_y a) \\ &- 2t_3[\cos(2p_x a) + \cos(2p_y a)] \\ &- 2t_4\cos(p_z d) - \mu,\end{aligned} \tag{41}$$

and to neglect the orbital effect of the magnetic field. Hereafter, the Hamiltonian $\mathcal{H}' = \mathcal{H}'_0 + \mathcal{H}_{\rm SC} + \mathcal{H}_{\rm AFM}$ is used to obtain the free energy f_Δ, while we will avoid the GL expansion of f_Δ in the SC order parameter Δ. Due to the neglect of the orbital effect of the magnetic field, the SC order parameter in the FFLO phase can be assumed to be homogeneous (uniform), in the real space, in the plane perpendicular to the field so that we assume the form $\Delta(\mathbf{r}) = |\Delta|\sqrt{2}\cos(q_{\rm LO}\tilde{y})$ for the SC order parameter. Further, in our calculation in the Pauli limit, we have assumed the g factor to be isotropic because the anisotropy in the g factor merely leads to a trivial θ-dependent change of the scale of the magnetic field (see also below).

The normal and anomalous Green's functions in the Matsubara representation are defined as

$$\begin{aligned}G^{(\sigma)}(\tau;\mathbf{r}_1,\mathbf{r}_2) &= -\langle T_\tau[\psi^{(\sigma)}(\mathbf{r}_1,\tau)[\psi^{(\sigma)}]^\dagger(\mathbf{r}_2,0)]\rangle, \\ \overline{F}^{(\sigma)}(\tau;\mathbf{r}_1,\mathbf{r}_2) &= -\langle T_\tau[[\psi^{(-\sigma)}]^\dagger(\mathbf{r}_1,\tau)[\psi^{(\sigma)}]^\dagger(\mathbf{r}_2,0)]\rangle, \\ F^{(\sigma)}(\tau;\mathbf{r}_1,\mathbf{r}_2) &= -\langle T_\tau[\psi^{(\sigma)}(\mathbf{r}_1,\tau)\psi^{(-\sigma)}(\mathbf{r}_2,0)]\rangle, \\ \overline{G}^{(\sigma)}(\tau;\mathbf{r}_1,\mathbf{r}_2) &= -\langle T_\tau[[\psi^{(\sigma)}]^\dagger(\mathbf{r}_1,\tau)\psi^{(\sigma)}(\mathbf{r}_2,0)]\rangle,\end{aligned} \tag{42}$$

and the Nambu matrix notation

$$\hat{G}^{(\sigma)}(\tau;\mathbf{r}_1,\mathbf{r}_2) = \begin{bmatrix} G^{(\sigma)}(\tau;\mathbf{r}_1,\mathbf{r}_2) & F^{(\sigma)}(\tau;\mathbf{r}_1,\mathbf{r}_2) \\ \overline{F}^{(\sigma)}(\tau;\mathbf{r}_1,\mathbf{r}_2) & \overline{G}^{(-\sigma)}(\tau;\mathbf{r}_1,\mathbf{r}_2)\end{bmatrix} \tag{43}$$

will be used. The Fourier component $\hat{G}^{(\sigma)}_{\varepsilon_n}(\mathbf{p};\mathbf{R}) \equiv \int d\tau\, e^{i\varepsilon_n\tau}\int d^3(\mathbf{r}_1-\mathbf{r}_2)\hat{G}^{(\sigma)}(\tau;\mathbf{r}_1,\mathbf{r}_2)e^{-i\mathbf{p}\cdot(\mathbf{r}_1-\mathbf{r}_2)}$ is represented as

$$\begin{bmatrix} i\varepsilon_n - \varepsilon(\mathbf{p}+\partial_{\mathbf{R}}) + \sigma I & -\sigma\Delta_{\mathbf{p}}(\mathbf{R}) \\ \sigma\Delta^*_{\mathbf{p}}(\mathbf{R}) & -i\varepsilon_n - \varepsilon(\mathbf{p}+\partial_{\mathbf{R}}) - \sigma I\end{bmatrix} \times \hat{G}^{(\sigma)}_{\varepsilon_n}(\mathbf{p};\mathbf{R}) = \hat{1} \tag{44}$$

with $\mathbf{R} = (\mathbf{r}_1 + \mathbf{r}_2)/2$. The Green's functions are expanded as a power series in the gradient $\nabla_{\mathbf{R}}$ and expressed as

$\hat{G}^{(\sigma)} = \hat{G}^{(\sigma)}_{(0)} + \hat{G}^{(\sigma)}_{(2)} + \hat{G}^{(\sigma)}_{(4)} + \ldots$ where

$$\hat{G}^{(\sigma)}_{\varepsilon_n,(0)}(\mathbf{p};\mathbf{R}) = \begin{bmatrix} i\varepsilon_n - \varepsilon(\mathbf{p}) + \sigma I & -\sigma\Delta_{\mathbf{p}}(\mathbf{R}) \\ \sigma\Delta^*_{\mathbf{p}}(\mathbf{R}) & -i\varepsilon_n - \varepsilon(\mathbf{p}) - \sigma I \end{bmatrix}^{-1} = \frac{1}{\varepsilon(\mathbf{p})^2 - (i\varepsilon_n + \sigma I)^2 + |\Delta_{\mathbf{p}}(\mathbf{R})|^2} \times \begin{bmatrix} -i\varepsilon_n - \varepsilon(\mathbf{p}) - \sigma I & \sigma\Delta_{\mathbf{p}}(\mathbf{R}) \\ -\sigma\Delta^*_{\mathbf{p}}(\mathbf{R}) & i\varepsilon_n - \varepsilon(\mathbf{p}) + \sigma I \end{bmatrix}, \tag{45}$$

$$\hat{G}^{(\sigma)}_{\varepsilon_n,(2)}(\mathbf{p},\mathbf{R}) = \hat{G}^{(\sigma)}_{(0)}\big[\mathbf{v}_{\mathbf{p}}\cdot\partial_{\mathbf{R}}\big(\hat{G}^{(\sigma)}_{(0)}\mathbf{v}_{\mathbf{p}}\cdot\partial_{\mathbf{R}}\hat{G}^{(\sigma)}_{(0)}\big)\big],$$

$$\hat{G}^{(\sigma)}_{\varepsilon_n,(4)}(\mathbf{p},\mathbf{R}) = \hat{G}^{(\sigma)}_{(0)}\big(\mathbf{v}_{\mathbf{p}}\cdot\partial_{\mathbf{R}}\big\{\hat{G}^{(\sigma)}_{(0)}\mathbf{v}_{\mathbf{p}}\cdot\partial_{\mathbf{R}}\big[\hat{G}^{(\sigma)}_{(0)}\mathbf{v}_{\mathbf{p}}\cdot\partial_{\mathbf{R}} \times \big(\hat{G}^{(\sigma)}_{(0)}\mathbf{v}_{\mathbf{p}}\cdot\partial_{\mathbf{R}}\hat{G}^{(\sigma)}_{(0)}\big)\big]\big\}\big), \tag{46}$$

$$\partial_{\mathbf{R}} = \begin{cases} \Pi = -i\nabla_{\mathbf{R}} - 2e\mathbf{A}(\mathbf{R}) & \text{for } \Delta(\mathbf{R}), \\ \Pi^\dagger = -i\nabla_{\mathbf{R}} + 2e\mathbf{A}(\mathbf{R}) & \text{for } \Delta^*(\mathbf{R}), \\ -i\nabla_{\mathbf{R}} & \text{otherwise.} \end{cases} \tag{47}$$

The mean field free energy associated with the SC order can be constructed in the way[36]

$$f_\Delta(q_{\mathrm{LO}}) = \left\langle \frac{|\Delta(\mathbf{R})|^2}{|g|} + \frac{T}{2}\sum_{\varepsilon_n=-\infty}^{\infty}\sum_{\mathbf{p},\sigma}\int_{\varepsilon_n}^{\infty s_\epsilon} d\omega\ \mathrm{Tr}\big[i\hat{\sigma}_z\hat{G}^{(\sigma)}_{\omega}(\mathbf{p},\mathbf{R})\big]\right\rangle_{\mathrm{sp}}. \tag{48}$$

By using the relations (45) to (48), the free-energy functional is expanded as a power series in the gradient $\nabla_{\mathbf{R}}$ and in the AFM order parameter m and takes the form

$$f_\Delta = f_\Delta(q_{\mathrm{LO}}) + f_m = f_{\Delta,(0)} + f_{\Delta,(2)} + f_{\Delta,(4)} + \ldots + f^{(2)}_m + f^{(4)}_m + \ldots. \tag{49}$$

The concrete expression of each $f_{\Delta,(n)}$ expressing the nth-order term in the gradient is

$$f_{\Delta,(0)} = \left\langle \frac{|\Delta(\mathbf{R})|^2}{|g|} - T\sum_{\varepsilon_n>0}\sum_{\mathbf{p}}\ln\left[\frac{\{\varepsilon_n^2 + [\varepsilon(\mathbf{p})]^2 + |\Delta_{\mathbf{p}}(\mathbf{R})|^2 - I^2\}^2 + 4\varepsilon_n^2 I^2}{\{\varepsilon_n^2 + [\varepsilon(\mathbf{p})]^2 - I^2\}^2 + 4\varepsilon_n^2 I^2}\right]\right\rangle_{\mathrm{sp}},$$

$$f_{\Delta,(2)} = \left\langle T\sum_{\varepsilon_n>0}\sum_{\mathbf{p}}\left[\frac{a_1^2 - b_1^2}{(a_1^2+b_1^2)^2}|\mathbf{v}_{\mathbf{p}}\cdot\Pi\Delta_{\mathbf{p}}(\mathbf{R})|^2 + \frac{2}{3}\frac{\{2[\varepsilon(\mathbf{p})]^2 - \varepsilon_n^2 + I^2 - |\Delta_{\mathbf{p}}(\mathbf{R})|^2\}(a_1^4 - 6a_1^2b_1^2 + b_1^4) - 4a_1b_1^2(a_1^2 - b_1^2)}{(a_1^2+b_1^2)^4} \times [\mathbf{v}_{\mathbf{p}}\cdot\nabla|\Delta_{\mathbf{p}}(\mathbf{R})|^2]^2\right]\right\rangle_{\mathrm{sp}},$$

$$f_{\Delta,(4)} \simeq \left\langle \frac{2T}{3}\sum_{\varepsilon_n>0}\sum_{\mathbf{p}}\left[\frac{\{2[\varepsilon(\mathbf{p})]^2 - \varepsilon_n^2 + I^2 - |\Delta_{\mathbf{p}}(\mathbf{R})|^2\}(a_1^4 - 6a_1^2b_1^2 + b_1^4) - 4a_1b_1^2(a_1^2 - b_1^2)}{(a_1^2+b_1^2)^4}|(\mathbf{v}_{\mathbf{p}}\cdot\Pi)^2\Delta_{\mathbf{p}}(\mathbf{R})|^2\right]\right\rangle_{\mathrm{sp}}, \tag{50}$$

respectively, where $a_1 = [\varepsilon(\mathbf{p})]^2 + \varepsilon_n^2 + |\Delta_{\mathbf{p}}(\mathbf{R})|^2 - I^2$, and $b_1 = 2\varepsilon_n I$. On the other hand, the terms $f^{(2)}_m$ and $f^{(4)}_m$ describing the mean field AFM ordering are expressed as

$$f^{(2)}_m = \left\langle\left[\frac{1}{U} + \frac{T}{2}\sum_{\varepsilon_n=-\infty}^{\infty}\sum_{\mathbf{p},\sigma}\mathrm{Tr}\left(\sum_{j=1}^{2}A_j\hat{a}_j\hat{G}^{(\sigma)}_{\varepsilon_n,(0)}(\mathbf{p};\mathbf{R})\hat{b}_j\hat{G}^{(\alpha_j)}_{\varepsilon_n,(0)}(\mathbf{p}+\mathbf{Q}_0+\mathbf{q};\mathbf{R})\right)\right]|m(\mathbf{R})|^2\right\rangle_{\mathrm{sp}},$$

$$f^{(4)}_m = \left\langle\frac{T}{4}\sum_{\varepsilon_n=-\infty}^{\infty}\sum_{\mathbf{p},\sigma}\mathrm{Tr}\left(\sum_{j=1}^{5}A''_j\hat{a}''_j\hat{G}^{(\sigma)}_{\varepsilon_n,(0)}(\mathbf{p};\mathbf{R})\hat{b}''_j\hat{G}^{(\alpha''_j)}_{\varepsilon_n,(0)}(\mathbf{p}+\mathbf{Q}_0+\mathbf{q};\mathbf{R})\hat{c}''_j\hat{G}^{(\beta''_j)}_{\varepsilon_n,(0)}(\mathbf{p};\mathbf{R})\hat{d}''_j\hat{G}^{(\gamma''_j)}_{\varepsilon_n,(0)}(\mathbf{p}+\mathbf{Q}_0+\mathbf{q};\mathbf{R})\right)|m(\mathbf{R})|^4\right\rangle_{\mathrm{sp}}, \tag{51}$$

and the coefficients $A_j, \alpha_j, \hat{a}_j, \hat{b}_j, A''_j, \alpha''_j, \beta''_j, \gamma''_j, \hat{a}''_j, \hat{b}''_j, \hat{c}''_j$, and $\hat{d}''_j$ are represented in Tables IV and V.

Finally, the concrete expressions of the free energy $f^{(2)}_m$ and $f^{(4)}_m$ in Eq. (51) are represented by

$$f^{(2)}_m = \left\langle\left[\frac{1}{U} + 2T\sum_{\varepsilon_n>0}\sum_{\mathbf{p}}\left(\sum_{j=1}^{2}A_jV^{(2)}_{m,j}(\mathbf{p},\mathbf{q};\mathbf{R})\right)\right] \times |m(\mathbf{R})|^2\right\rangle_{\mathrm{sp}},$$

$$f^{(4)}_m = \left\langle T\sum_{\varepsilon_n>0}\sum_{\mathbf{p}}\left(\sum_{j=1}^{5}A''_jV^{(4)}_{m,j}(\mathbf{p},\mathbf{q};\mathbf{R})\right)|m(\mathbf{R})|^4\right\rangle_{\mathrm{sp}}, \tag{52}$$

where the details of $V^{(2)}_{m,j}$ and $V^{(4)}_{m,j}$ will be given in the Appendix.

A. Results

Now, numerically obtained results on the phase diagram will be explained in the following. Figures 4(a)–4(d) show field versus temperature (H-T) phase diagrams including the

TABLE IV. Coefficients α_j, A_j, B_j in Eq. (51).

j	α_j	A_j	$\hat{a}_j$	$\hat{b}_j$
1	$-\sigma$	$\cos^2\theta$	$\hat{1}$	$\hat{1}$
2	σ	$\sin^2\theta$	$\hat{\sigma}_z$	$\hat{\sigma}_z$

TABLE V. Coefficients α''_j, β''_j, γ''_j, A''_j, $\hat{a}''_j$, $\hat{b}''_j$, $\hat{c}''_j$, $\hat{d}''_j$ in Eq. (51).

j	α''_j	β''_j	γ''_j	A''_j	$\hat{a}''_j$	$\hat{b}''_j$	$\hat{c}''_j$	$\hat{d}''_j$
1	$-\sigma$	σ	$-\sigma$	$\cos^4\theta$	$\hat{1}$	$\hat{1}$	$\hat{1}$	$\hat{1}$
2	σ	σ	σ	$\sin^4\theta$	$\hat{\sigma}_z$	$\hat{\sigma}_z$	$\hat{\sigma}_z$	$\hat{\sigma}_z$
3	σ	σ	$-\sigma$	$2\cos^2\theta\sin^2\theta$	$\hat{1}$	$\hat{\sigma}_z$	$\hat{\sigma}_z$	$\hat{1}$
4	σ	$-\sigma$	σ	$2\cos^2\theta\sin^2\theta$	$\hat{\sigma}_z$	$\hat{\sigma}_z$	$\hat{1}$	$\hat{1}$
5	σ	$-\sigma$	$-\sigma$	$-2\cos^2\theta\sin^2\theta$	$\hat{1}$	$\hat{\sigma}_z$	$\hat{1}$	$\hat{\sigma}_z$

PPB-induced AFM and FFLO orders obtained at some fixed angles and in the Pauli limit with no orbital pair breaking. In each figure, the thick solid (black) curve denotes the first-order H_{c2} transition line, and the dotted (red) one denotes the second-order transition line separating the FFLO phase from the uniform SC (U) phase corresponding to the ordinary Abrikosov lattice. For $\theta \leqslant 20^\circ$, the AFM transition occurring on the dashed (blue) curve is also of second order (see, however, Fig. 7). The additional solid (green) curve lying below the H_{c2} line in (a) denotes a transition line separating the two different AFM-FFLO coupled structures shown in Fig. 1 from each other. As examined in Ref. 14, in the parallel fields case shown in Fig. 4(a), AFM order tends to appear just in the FFLO phase because AFM order is induced by PPB effects and, in addition, is stabilized by taking a spatial modulation commensurate to the FFLO modulation parallel to the magnetic field. However, the relative phase between the spatial modulations of AFM and FFLO may be changed depending upon the field strength. As Fig. 4(a) shows, the AFM order favors coexistence [i.e, the structure of Fig. 1(a)] with the nonvanishing SC order in real space in higher fields, which is a feature consistent with the NMR data,[8] and a structural transition is expected to occur on the additional solid (green) curve with decreasing the field in the HFLT phase.

The resulting angular dependence of the AFM-ordered region in this Pauli-limited model is similar to that in the preceding section. With tilting the field away from the superconducting plane, the nesting condition for the AFM ordering becomes gradually unsatisfactory because the magnetic field component parallel to the AFM moment $\mathbf{m} \parallel c$ (Refs. 11, 12, and 27) is increased by the tilt so that the incommensurate AFM wave vectors for different spin components do not coincide with each other when $\theta \neq 0^\circ$. Therefore, as shown in Fig. 4(b), AFM order tends to be suppressed by the tilt even without the orbital pair breaking. However, the primary origin of this AFM order in the SC order, i.e., the PPB effect, is enhanced with increasing the field. Due to a competition between this field-induced enhancement of PPB and the above-mentioned less complete nesting condition due to the field tilt, the

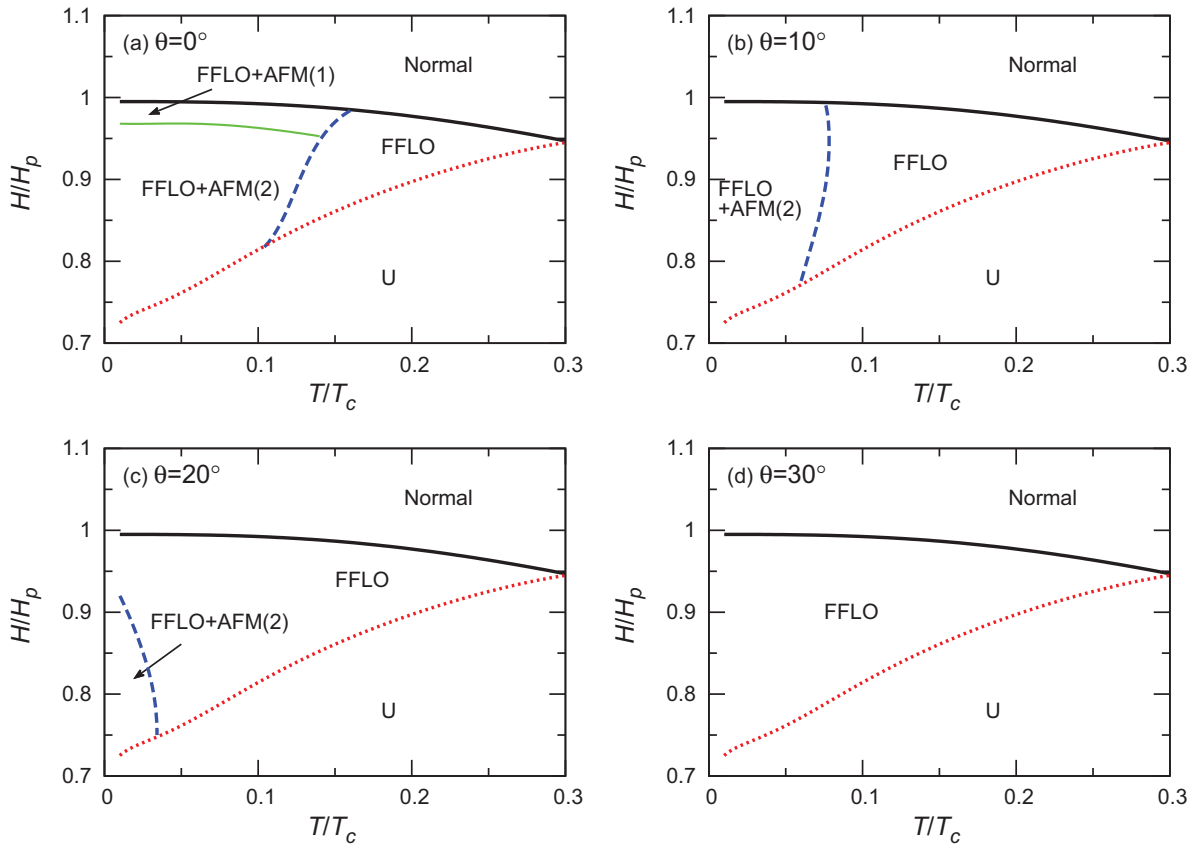

FIG. 4. (Color online) Angular dependence of the H-T phase diagrams in the Pauli limit. In this calculation, the parameter values $T_c/U = 0.01597$, $t_1/T_c = 15$, $t_2/t_1 = -1.5$, $t_3/t_1 = 0.65$, $t_4/t_1 = 0.5$, and $\mu/t_1 = 1.85$ are used. In each of the four figures, the thin solid (green) line in (a) denotes a structural transition on the relative configuration between the spatially modulated AFM order and the FFLO one (see the text), while the remaining curves are defined in the same manner as those in Fig. 3. The uniform SC (U) phase corresponds to the Abrikosov lattice (A) in Fig. 3, i.e., the case including the orbital pair breaking.

resulting AFM phase is pushed down to *lower* fields within the FFLO phase. Thus, the pure (nonmagnetic) FFLO state appears between the AFM-ordered region and the H_{c2} line. In contrast to the GL approach in the preceding section, we have not assumed an anisotropy of the g factor. For this reason, the resulting H_{c2} curve in Fig. 4 is independent of the angle. A more realistic angular dependence of the H-T phase diagram in the Pauli limit is trivially obtained by properly changing the scale of the ordinate of the Figs. 4(b) to 4(d). It is remarkable that, nevertheless, the real-space structure of the AFM order is highly sensitive to the field tilt: The in-phase structure, FFLO + AFM(1) in the figure (a), [i.e., Fig. 1(a)], seen in the parallel field case is lost by a small tilt of the field, and the resulting AFM order for $\theta \neq 0^\circ$ basically takes the out-of-phase structure [FFLO + AFM(2)] defined in Fig. 1(b). It seems that a weaker AFM ordering leads to the out-of-phase structure in which the AFM order appears in the region where the SC energy gap vanishes.

We need to stress that the out-of-phase configuration [Fig. 1(b)] of the AFM order is realized in many situations in the present Pauli limit in contrast to the fact that only the in-phase configuration [Fig. 1(a)] is realized in Sec. II where the orbital pair-breaking effect is also included. The origin of such a difference in the AFM spatial configuration *parallel* to **H** consists in the GL expansion in powers of Δ used in the preceding section. The main contribution to the free-energy density necessary for obtaining the PPB-induced AFM order is Eq. (35) in the GL approach in Sec. II, or equivalently the anomalous term in the susceptibility $-\chi^{(an)}$ in Refs. 13 and 14. We note that, in the Pauli limit in the present section, the $-\chi^{(an)}$ contribution is included in $f_m^{(2)}$. Then, let us consider such a coupling term corresponding to $-\chi^{(an)}$ in the following simplified form:

$$f_{\rm cp}(\mathbf{r}) = -C_{\rm cp}\frac{|\Delta(\mathbf{r})|^2|\mathbf{m}(\mathbf{r})|^2}{1+D_{\rm cp}|\Delta(\mathbf{r})|^2}, \tag{53}$$

where the **r**-independent coefficients $C_{\rm cp}$ and $D_{\rm cp}$ are positive. The GL approach is valid for small enough $D_{\rm cp}$ values. Then, substituting Eqs. (11) and (14) into Eq. (53), it is readily seen that the in-phase configuration [Fig. 1(a)] is more stable. In contrast, in the situation deep in the SC state where the GL approach is not effective, the coefficient $D_{\rm cp}$ may have a substantial magnitude. For brevity, if considering the limit of a large $D_{\rm cp}$, the energy gain due to $f_{\rm cp}$ in the in-phase configuration is suppressed by an increase of the denominator in Eq. (53), and the out-of-phase configuration is rather stabilized. In this manner, it is understood why the in-phase configuration is realized in higher fields near H_{c2}. Further, since the field tilt destabilizes the AFM order closer to H_{c2}, it is understood why the out-of-phase configuration of the AFM order becomes more dominant in the HFLT phase with tilting the field from the a-b plane.

Here, we discuss the angular dependence of the resulting AFM wave vector consistent with the phase diagrams Fig. 4. In a previous work[14] focusing on the parallel field configuration $\mathbf{H} \perp c$, we have shown how the AFM wave vector insensitive to the field[11,12] is explained within the present approach. Below, we explain how the AFM wave vector insensitive even to the tilt angle[27] follows from the present theory. To do this, we present Fig. 5(a) showing the projection of the Fermi surface (FS) onto the p_x-p_y plane. In the present case with a component of the magnetic field parallel to the AFM momemt ($\parallel c$), a Zeeman splitting of the AFM wave vector occurs. That is, the wave vector $\mathbf{q}_\uparrow$ satisfying the nesting condition for the up-spin quasiparticles is different from the corresponding one $\mathbf{q}_\downarrow$ for the down-spin quasiparticle. It is easily seen that $|\mathbf{q}_\uparrow| > |\mathbf{q}_\downarrow|$ (see Fig. 5). In Fig. 5(a), the solid red (blue) curve denotes FS of up- (down-) spin quasiparticles, while the red (blue) arrow represents $\mathbf{Q}_0 - \mathbf{q}_\uparrow$ ($\mathbf{Q}_0 - \mathbf{q}_\downarrow$) vector projected onto the p_x-p_y plane, respectively. In Fig. 5(b), FSs projected on the $p_x(=p_y)$-p_z plane are indicated by the solid curves, and the dashed red (blue) curve denotes the $\mathbf{q}_\uparrow$ shift ($\mathbf{q}_\downarrow$ shift) of each FS, and the red (blue) arrow there represents the

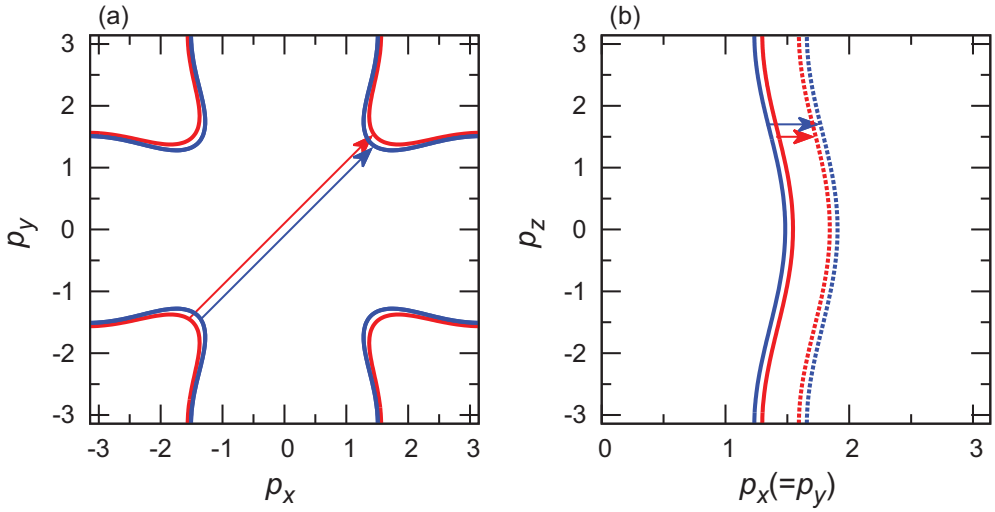

FIG. 5. (Color online) Fermi surface (FS) of the p_x-p_y plane (a) and $p_y(=p_x)$-p_z plane (b) obtained from the dispersion relation (41), where the parameters $t_1/T_c = 15$, $t_2/t_1 = -1.5$, $t_3/t_1 = 0.65$, $t_4/t_1 = 0.5$, and $\mu/t_1 = 1.85$ were used, and the $c(=\hat{z})$ axis was chosen as the spin-quantization axis. The FS for up-spin and down-spin quasiparticles is described as a red solid and blue solid curve, respectively. The red (blue) arrow in (a) represents the $\mathbf{Q}_0 - \mathbf{q}_\uparrow$ ($\mathbf{Q}_0 - \mathbf{q}_\downarrow$) vector projected in the p_x-p_y plane, while the red (blue) arrow in (b) represents the $\mathbf{q}_\uparrow$ ($\mathbf{q}_\downarrow$) vector projected in the p_y-p_z plane. With increasing the Zeeman splitting, $|\mathbf{q}_\uparrow|$ ($|\mathbf{q}_\downarrow|$) becomes smaller (larger).

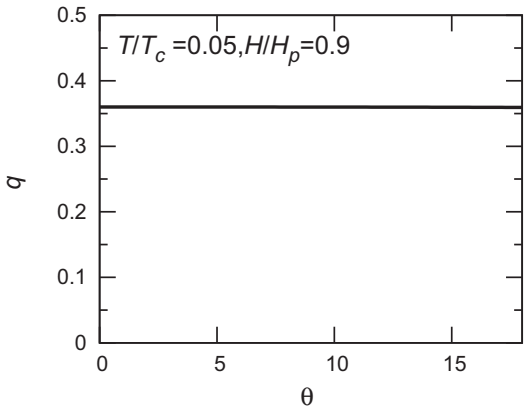

FIG. 6. Angular dependence of the incommensurate vector **q** resulting from the FS at $T/T_c = 0.05$ and $H/H_P = 0.9$. The decrease of **q** by tilting the field is very small below $\theta = 20^\circ$ and $|\mathbf{q}|$ is seemingly independent of the angle. This feature is consistent with the experimental fact (Ref. 27).

corresponding projection of $\mathbf{q}_\uparrow$ ($\mathbf{q}_\downarrow$), respectively. This figure shows that the distortion of FS along the c direction does not affect the direction of the incommensurate wave vector.

In this calculation, we find that the AFM structure with lower free energy is reached by assuming that, reflecting the difference in the density of states between the up-spin and down-spin quasiparticles, $\mathbf{Q}_0 - \mathbf{q}_\uparrow$ plays the role of the AFM wave vector to be realized. Thus, hereafter the structure of the AFM order will be discussed based on this choice of **q**. Figure 6 shows an example of the resulting angular dependence of the incommensurate wave vector $|\mathbf{q}|$. In general, we find that $|\mathbf{q}|$ decreases as θ is larger. However, the extent of the decrease is quite small in $|\theta| < 20^\circ$ where the AFM order is realized. Therefore, $|\mathbf{q}|$ is seemingly independent of the angle. We note that, in the neutron diffraction measurements[27] performed in the tilted configuration, $|\mathbf{q}|$ has been insensitive to the tilt angle of the magnetic field from the a-b plane. At this stage, however, we can not exclude the possibility that this consistency with the experimental data[27] may be based largely on the local approximation used in this work (see Sec. II).

We note that, in the present Pauli-limited model, the FFLO order is not suppressed sufficiently by the field tilt. This seemingly inconsistent behavior with experimental facts is a result of our neglect in this model of the orbital pair-breaking effect. As seen in the preceding section, inclusion of the orbital pair-breaking effect recovers a tilt-induced reduction[28–30] of the FFLO-ordered region.

Before ending this section, the character of the AFM transition in the HFLT phase will be discussed when $\theta \neq 0^\circ$. As already mentioned, the nonmagnetic FFLO region with no AFM order inevitably appears even in the parallel field ($\theta = 0^\circ$) case in the present approach neglecting the AFM *fluctuation*, and the character of the resulting AFM transition in the HFLT phase is of second order.[13,14] As shown in Fig. 7(a), this second-order character is maintained for a smaller $\theta \neq 0^\circ$ and/or in the high-temperature side of the HFLT phase. However, at low enough temperatures and/or at larger tilt angles ($\theta > 20^\circ$), this transition is nearly of first order, as seen in Fig. 7(b). In fact, such a sharp vanishing of the AFM moment at a higher field in the HFLT phase has been seen in the recent NMR data in $\theta \neq 0$.[30]

IV. SUMMARY

In this paper, we have investigated, within the mean field approximation, how the high-field low-temperature (HFLT) SC phase found in $CeCoIn_5$ in the parallel field configuration is changed by rotating (or tilting) the field direction from the basal plane. Since it is difficult at present to perform a complete analysis incorporating various features of the ordered states due to PPB effects on the same footing, we have examined two models separately to obtain basic knowledge on the present issue. In one model, we have incorporated the orbital pairing breaking, i.e., the presence of the vortices, while, instead, the GL expansion in the SC order parameter Δ has been assumed. Due to the use of the GL expansion in Δ, the relative structure

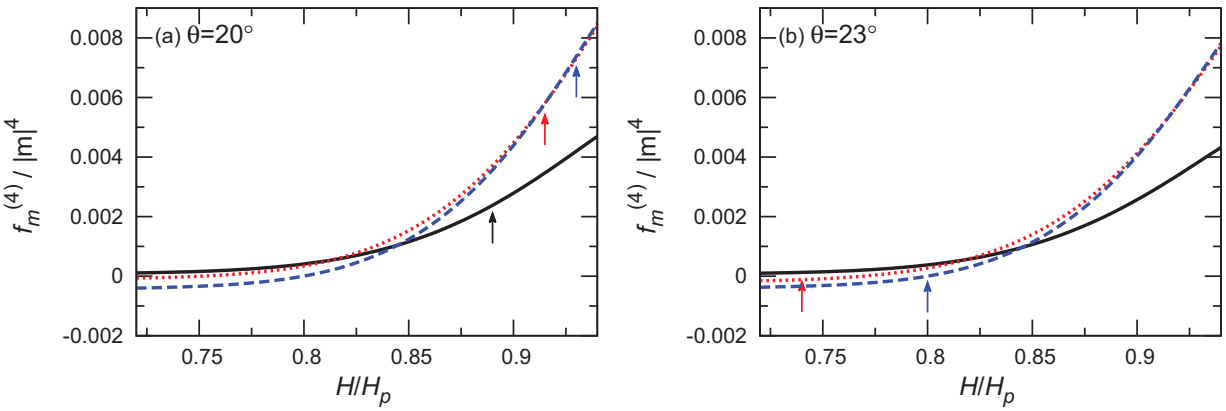

FIG. 7. (Color online) Field dependence of the coefficient of the quartic term in the AFM order parameter $|m|$, defined as the ratio $f_m^{(4)}/|m|^4$ at the reduecd temperature $t = 0.02$ (black), 0.01 (red), and 0.005 (blue) and for (a) $\theta = 20^\circ$ and (b) 23°. On each curve, the AFM transition field is indicated by an arrow with the corresponding color by assuming the transition to be of second order. Thus, if, as in the figure (b), $f_m^{(4)}/|m|^4$ is negative at the (assumed) AFM transition field, the real AFM transition should be a discontinuous or a nearly discontinuous one. Although our results on this quantity suggest that the AFM transition in the HFLT phase tends to become of first order with tilting the field in $\theta < 30^\circ$, this does not necessarily imply the absence of a quantum critical behavior in $\mathbf{H} \parallel c$.

in real space between the resulting AFM order and the FFLO modulation is found not to become consistent with the recent experimental data.[30] Instead, we have found such a feature consistent with the experimental data[28,29] that the field range of the HFLT phase, identified with the FFLO state itself, in the H-T phase diagram is significantly reduced with tilting the field because the orbital pair breaking included in this GL approach becomes more important, due to the uniaxial crystalline anisotropy, with tilting the field.

On the other hand, to improve our understanding on the details of the resulting AFM order in real space, we have also examined the Pauli-limited model, in which Δ is uniform in the plane perpendicular to the field due to the neglect of the orbital pair breaking, while the GL expansion in Δ is not assumed. Due to the neglect of the orbital pair breaking, the FFLO ordering is overestimated in this model, and the correct angular dependence of the FFLO region is not obtained. Instead, reflecting higher-order couplings between the AFM and SC order parameters which are absent in the GL approach in Sec. II, both of the two different configurations, illustrated in Fig. 1, of the AFM and FFLO structures parallel to the field are obtained in the parallel field configuration with a field dependence qualitatively consistent with the data.[8]

The main result in this work is the angular dependence of the AFM-ordered region in the FFLO phase found *commonly* both in our two models in the preceding two sections. Originally, an increase of the magnetic field enhances PPB effects, i.e., the present AFM ordering, while the c-axis component of the magnetic field induced by tilting the field direction from the basal plane makes the nesting condition for the AFM unsatisfactory as far as the AFM moment is parallel to the c axis.[11,12,27] These two competitive roles of the tilted magnetic field for the AFM ordering shift the field range, in which the AFM ordering is maximal, to lower fields than $H_{c2}(0)$. Consequently, when tilting the field, the AFM order is first lost in the *high*-field range just below the $H_{c2}(T)$ line. This strikingly coincides with the feature seen through a NMR measurement[30] in the angular dependence of the AFM-ordered region in the HFLT phase of $CeCoIn_5$. In addition, this type of reduction of the AFM order suggests that, at higher tilt angles, a remaining AFM quantum critical point (AFM-QCP) should lie at a slightly lower field than $H_{c2}(0)$. This expected position of the AFM-QCP seems to be consistent with the experimental facts[16,31] in $\mathbf{H} \parallel c$ which show an AFM-QCP not coinciding with $H_{c2}(0)$ but lying clearly below it. Further, we have found, in the Pauli limit where the GL expansion in Δ is not used, that inclusion of an effect suppressing the AFM ordering in the FFLO state, such as the field tilt, results in the formation of the AFM order close to the FFLO nodal planes. It means that, as seen in Figs. 4(b)–4(d), a field tilt from the in-plane field configuration results in the structure illustrated in Fig. 1(b) in contrast to the high-field behavior in the in-plane field configuration seen in Fig. 4(a). This change on the AFM ordering by the field tilt has also been found in recent NMR data on the angular dependence of the HFLT phase of $CeCoIn_5$.[30]

The present theory on the high-field AFM ordering in superconductors with strong PPB is the first study on the angular (θ) dependence of the HFLT SC phase found in $CeCoIn_5$. Further, even if focusing on the parallel field case with $\theta = 0$, this is different from other works.[23–25] First of all, our works take account of correlation between the AFM and the FFLO orders, while just the AFM order has been considered as a consequence of PPB elsewhere.[24,25] We stress that the region with no AFM order *in the HFLT SC phase* has been realized at least by the field tilt.[30] Second of all, our works explain coexistence of the AFM order and the nonvanishing SC order parameter in real space which has been seen in the higher half of the field range of the HFLT phase in $\theta = 0$,[8] while the picture in Ref. 23 requires the resulting AFM order at any field-tilt angle to, as in Fig. 1(b), localize close to the FFLO nodal plane.

Finally, we should comment on the local approximation used to simplify our treatment. Effects of the FFLO order on the AFM order are incorporated even in this approximation. However, as explained in the text of Sec. II, in this local approximation, the couplings between the AFM and the SC orders of higher orders in the FFLO wave number $|q_{LO}|$ are neglected. This higher-order coupling would describe possible effects of the AFM order on the FFLO order and thus, on the $H_{c2}(T)$ curve at low temperatures. In addition, as mentioned in Sec. III, it is possible that the incommensurate AFM wave vector *insensitive* to the angle of the applied field might be largely due to the use of this approximation. Further study including these higher-order couplings will be reported elsewhere.

ACKNOWLEDGMENTS

We thank K. Aoyama for his contribution on the early stage of this work and discussions, and Y. Hatakeyama and K. Kumagai for discussions. This work is supported by Grant-in-Aid for Scientific Research (Grant No. 25400368) from MEXT, Japan.

APPENDIX

The GL free-energy functional in Eq. (21) can be obtained simply by extending the previous analysis[4,34] to the present tilted case, and its each term is given by

$$f_{\Delta}^{(2,0)} = N(0)T_c^2 \left\{ \frac{1}{2} \ln\left(\frac{H}{H_{\rm orb}^{\rm 2D}(0)}\right) + \int_0^{\infty} d\rho \left[\frac{1}{\rho} \exp\left(-\frac{\pi^2 \xi_0^2}{r_H^2}\rho^2\right) - f(\rho,\rho) \left\langle |w_{\mathbf{p}}|^2 \exp\left(-\frac{1}{2}|\mu|^2\rho^2\right)\right\rangle_{\rm FS} \right] \right\} \left(\frac{|\Delta|}{T_c}\right)^2,$$

$$f_{\Delta}^{(2,2)} = \frac{N(0)T_c^2}{2} \int_0^{\infty} d\rho\, f(\rho,\rho)\rho^2 \left\langle |w_{\mathbf{p}}|^2 \left(\frac{\tilde{v}_{\tilde{p},\tilde{y}}}{v_{\rm F}}\right)^2 \exp\left(-\frac{1}{2}|\mu|^2\rho^2\right)\right\rangle_{\rm FS} \left(\frac{|\Delta|}{T_c}\right)^2 \left(\frac{v_{\rm F}}{T_c}\right)^2,$$

$$
\begin{aligned}
f_{\Delta}^{(2,4)} &= -\frac{N(0)T_c^2}{24}\int_0^{\infty} d\rho\, f(\rho,\rho)\rho^4\left\langle |w_{\mathbf{p}}|^2\left(\frac{\tilde{v}_{\tilde{p},\tilde{y}}}{v_{\mathrm{F}}}\right)^4 \exp\left(-\frac{1}{2}|\mu|^2\rho^2\right)\right\rangle_{\mathrm{FS}}\left(\frac{|\Delta|}{T_c}\right)^2\left(\frac{v_{\mathrm{F}}}{T_c}\right)^4,\\
f_{\Delta}^{(4,0)} &= \frac{3N(0)T_c^2}{2}\int_0^{\infty}\prod_{i=1}^{3} d\rho_i\, f\left(\sum_{i=1}^{3}\rho_i,\sum_{i=1}^{3}\rho_i\right)\left\langle |w_{\mathbf{p}}|^4 \exp\left[-\frac{1}{2}\left(R_{14}-\frac{1}{2}R_{24}\right)\right]\cos(I_4)\right\rangle_{\mathrm{FS}}\left(\frac{|\Delta|}{T_c}\right)^4,\\
f_{\Delta}^{(4,2)} &= -\frac{3N(0)T_c^2}{4}\int_0^{\infty}\prod_{i=1}^{3} d\rho_i\, f\left(\sum_{i=1}^{3}\rho_i,\sum_{i=1}^{3}\rho_i\right)\left[\sum_{i=1}^{3}\rho_i^2-\frac{1}{3}\sum_{i\neq j}(-1)^{i+j}\rho_i\rho_j\right]\\
&\quad\times\left\langle |w_{\mathbf{p}}|^4\left(\frac{\tilde{v}_{\tilde{p},\tilde{y}}}{v_{\mathrm{F}}}\right)^2 \exp\left[-\frac{1}{2}\left(R_{14}-\frac{1}{2}R_{24}\right)\right]\cos(I_4)\right\rangle_{\mathrm{FS}}\left(\frac{|\Delta|}{T_c}\right)^4\left(\frac{v_{\mathrm{F}}}{T_c}\right)^2,\\
f_{\Delta}^{(4,4)} &= \frac{N(0)T_c^2}{16}\int_0^{\infty}\prod_{i=1}^{3} d\rho_i\, f\left(\sum_{i=1}^{3}\rho_i,\sum_{i=1}^{3}\rho_i\right)\left[\sum_{i=1}^{3}\rho_i^4+\sum_{i\neq j}\left[3\rho_i^2\rho_j^2-2(-1)^{i+j}\rho_i\rho_j(\rho_{6-i-j})^2-\frac{3}{4}(-1)^{i+j}\rho_i\rho_j^3\right]\right]\\
&\quad\times\left\langle |w_{\mathbf{p}}|^4\left(\frac{\tilde{v}_{\tilde{p},\tilde{y}}}{v_{\mathrm{F}}}\right)^4 \exp\left[-\frac{1}{2}\left(R_{14}-\frac{1}{2}R_{24}\right)\right]\cos(I_4)\right\rangle_{\mathrm{FS}}\left(\frac{|\Delta|}{T_c}\right)^4\left(\frac{v_{\mathrm{F}}}{T_c}\right)^4,\\
f_{\Delta}^{(6)} &= -\frac{5N(0)T_c^2}{2}\int_0^{\infty}\prod_{i=1}^{5} d\rho_i\, f\left(\sum_{i=1}^{5}\rho_i,\sum_{i=1}^{5}\rho_i\right)\left\langle |w_{\mathbf{p}}|^6 \exp\left[-\frac{1}{2}\left(R_{16}+R_{26}\right)\right]\cos(I_6)\right\rangle_{\mathrm{FS}}\left(\frac{|\Delta|}{T_c}\right)^6,
\end{aligned}
\tag{A1}
$$

where ξ_0 is the in-plane coherence length,

$$
\begin{aligned}
R_{14} &= |\mu|^2\left[\sum_{i=1}^{3}\rho_i^2+\rho_2(\rho_1+\rho_3)\right],\quad R_{24} = \mathrm{Re}(\mu^2)\left[\rho_2^2+(\rho_1-\rho_3)^2\right],\\
I_4 &= \frac{1}{4}\,\mathrm{Im}(\mu^2)\left[-\rho_2^2+(\rho_1-\rho_3)^2\right],\quad R_{16} = |\mu|^2\left(e_1+e_2+e_3+\frac{2}{3}e_4e_5\right),\\
R_{26} &= \mathrm{Re}(\mu^2)\left[e_1+e_2+e_3-\frac{e_4^2+e_5^2}{3}-\frac{2}{3}(e_6+e_7+e_8+e_9)\right],\\
I_6 &= \frac{1}{4}\mathrm{Im}(\mu^2)\left[e_1+e_2-e_3-\frac{e_4^2-e_5^2}{3}-\frac{2}{3}(e_6+e_7-e_8-e_9)\right],\\
e_1 &= (\rho_3+\rho_5)^2+(\rho_3+\rho_4)^2,\quad e_2 = (\rho_1+\rho_4+\rho_5)^2,\quad e_3 = \rho_3^2+\rho_4^2+(\rho_2-\rho_5)^2,\\
e_4 &= \rho_1+2(\rho_3+\rho_4+\rho_5),\quad e_5 = \rho_2-\rho_3-\rho_4-\rho_5,\quad e_6 = (\rho_4-\rho_5)^2+(\rho_1-\rho_3+\rho_5)^2,\\
e_7 &= (\rho_1-\rho_3+\rho_4)^2,\quad e_8 = (\rho_3-\rho_4)^2+(\rho_2+\rho_3-\rho_5)^2,\quad e_9 = (\rho_2+\rho_4-\rho_5)^2,
\end{aligned}
\tag{A2}
$$

$$
\begin{aligned}
V_{m,1}^{(2)}(\mathbf{p},\mathbf{q};\mathbf{R}) &= -\frac{2}{c_1^2+d_1^2}\left\{c_1\left[\varepsilon_n^2+I^2-\varepsilon(\mathbf{p})\varepsilon(\mathbf{p}+\mathbf{Q}_0+\mathbf{q})-\Delta_{\mathbf{p}}(\mathbf{R})\Delta^*_{\mathbf{p}+\mathbf{Q}_0+\mathbf{q}}(\mathbf{R})\right]\right\},\\
V_{m,2}^{(2)}(\mathbf{p},\mathbf{q};\mathbf{R}) &= -\frac{2}{c_2^2+d_2^2}\left\{c_2\left[\varepsilon_n^2-I^2-\varepsilon(\mathbf{p})\varepsilon(\mathbf{p}+\mathbf{Q}_0+\mathbf{q})-\Delta_{\mathbf{p}}(\mathbf{R})\Delta^*_{\mathbf{p}+\mathbf{Q}_0+\mathbf{q}}(\mathbf{R})\right]+d_2b_1\right\},\\
V_{m,1}^{(4)}(\mathbf{p},\mathbf{q};\mathbf{R}) &= \frac{2}{\left(c_1^2+d_1^2\right)^2}\left[\left(c_1^2-d_1^2\right)\left(\left[\varepsilon_n^2+I^2-\varepsilon(\mathbf{p})\varepsilon(\mathbf{p}+\mathbf{Q}_0+\mathbf{q})-\Delta_{\mathbf{p}}(\mathbf{R})\Delta^*_{\mathbf{p}+\mathbf{Q}_0+\mathbf{q}}(\mathbf{R})\right]^2\right.\\
&\quad-\varepsilon_n^2\{[\varepsilon(\mathbf{p})+\varepsilon(\mathbf{p}+\mathbf{Q}_0+\mathbf{q})]^2+|\Delta_{\mathbf{p}}(\mathbf{R})+\Delta_{\mathbf{p}+\mathbf{Q}_0+\mathbf{q}}(\mathbf{R})|^2\}+I^2\{[\varepsilon(\mathbf{p})-\varepsilon(\mathbf{p}+\mathbf{Q}_0+\mathbf{q})]^2\\
&\quad\left.+|\Delta_{\mathbf{p}}(\mathbf{R})-\Delta_{\mathbf{p}+\mathbf{Q}_0+\mathbf{q}}|^2\}-|\Delta_{\mathbf{p}}(\mathbf{R})\varepsilon(\mathbf{p}+\mathbf{Q}_0+\mathbf{q})-\Delta_{\mathbf{p}+\mathbf{Q}_0+\mathbf{q}}(\mathbf{R})\varepsilon(\mathbf{p})|^2\right)-2c_1d_1^2\Big],\\
V_{m,2}^{(4)}(\mathbf{p},\mathbf{q};\mathbf{R}) &= \frac{2}{\left(c_2^2+d_2^2\right)^2}\left[\left(c_2^2-d_2^2\right)\left(\left[\varepsilon_n^2-I^2-\varepsilon(\mathbf{p})\varepsilon(\mathbf{p}+\mathbf{Q}_0+\mathbf{q})-\Delta_{\mathbf{p}}(\mathbf{R})\Delta^*_{\mathbf{p}+\mathbf{Q}_0+\mathbf{q}}(\mathbf{R})\right]^2-b_1^2\right.\\
&\quad-\left(\varepsilon_n^2-I^2\right)\{[\varepsilon(\mathbf{p})+\varepsilon(\mathbf{p}+\mathbf{Q}_0+\mathbf{q})]^2+|\Delta_{\mathbf{p}}(\mathbf{R})+\Delta_{\mathbf{p}+\mathbf{Q}_0+\mathbf{q}}(\mathbf{R})|^2\}-|\Delta_{\mathbf{p}}(\mathbf{R})\varepsilon(\mathbf{p}+\mathbf{Q}_0+\mathbf{q})\\
&\quad\left.-\Delta_{\mathbf{p}+\mathbf{Q}_0+\mathbf{q}}(\mathbf{R})\varepsilon(\mathbf{p})|^2\right)-2c_2d_2b_1\{[\varepsilon(\mathbf{p})+\varepsilon(\mathbf{p}+\mathbf{Q}_0+\mathbf{q})]^2-2\left[\varepsilon_n^2-I^2-\varepsilon(\mathbf{p})\varepsilon(\mathbf{p}+\mathbf{Q}_0+\mathbf{q})\right]\\
&\quad+2\Delta_{\mathbf{p}}(\mathbf{R})\Delta^*_{\mathbf{p}+\mathbf{Q}_0+\mathbf{q}}(\mathbf{R})+|\Delta_{\mathbf{p}}(\mathbf{R})+\Delta_{\mathbf{p}+\mathbf{Q}_0+\mathbf{q}}(\mathbf{R})|^2\}\Big],\\
V_{m,3}^{(4)}(\mathbf{p},\mathbf{q};\mathbf{R}) &= \frac{2}{\left(a_2^2+b_1^2\right)\left(c_3^2+d_3^2\right)}\left[c_3\left(\left[\varepsilon_n^2+I^2-\varepsilon(\mathbf{p})\varepsilon(\mathbf{p}+\mathbf{Q}_0+\mathbf{q})-\Delta_{\mathbf{p}}(\mathbf{R})\Delta^*_{\mathbf{p}+\mathbf{Q}_0+\mathbf{q}}(\mathbf{R})\right]\right.\\
&\quad\times\left[\varepsilon_n^2-I^2-\varepsilon(\mathbf{p})\varepsilon(\mathbf{p}+\mathbf{Q}_0+\mathbf{q})-\Delta_{\mathbf{p}}(\mathbf{R})\Delta^*_{\mathbf{p}+\mathbf{Q}_0+\mathbf{q}}(\mathbf{R})\right]-\varepsilon_n^2\{[\varepsilon(\mathbf{p})+\varepsilon(\mathbf{p}+\mathbf{Q}_0+\mathbf{q})]^2
\end{aligned}
$$

$$
\begin{aligned}
&+|\Delta_{\mathbf{p}}(\mathbf{R})+\Delta_{\mathbf{p}+\mathbf{Q}_0+\mathbf{q}}(\mathbf{R})|^2\}-I^2[\varepsilon(\mathbf{p})^2-\varepsilon(\mathbf{p}+\mathbf{Q}_0+\mathbf{q})^2+|\Delta_{\mathbf{p}}(\mathbf{R})|^2-|\Delta_{\mathbf{p}+\mathbf{Q}_0+\mathbf{q}}(\mathbf{R})|^2]\\
&-|\Delta_{\mathbf{p}}(\mathbf{R})\varepsilon(\mathbf{p}+\mathbf{Q}_0+\mathbf{q})-\Delta_{\mathbf{p}+\mathbf{Q}_0+\mathbf{q}}(\mathbf{R})\varepsilon(\mathbf{p})|^2\big)\\
&+d_3b_1\big[\varepsilon_n^2+I^2-\epsilon(\mathbf{p}+\mathbf{Q}_0+\mathbf{q})^2-2\varepsilon(\mathbf{p})\varepsilon(\mathbf{p}+\mathbf{Q}_0+\mathbf{q})-|\Delta_{\mathbf{p}+\mathbf{Q}_0+\mathbf{q}}(\mathbf{R})|^2-2\Delta_{\mathbf{p}}(\mathbf{R})\Delta^*_{\mathbf{p}+\mathbf{Q}_0+\mathbf{q}}(\mathbf{R})\big]\big],
\end{aligned}
$$

$$
\begin{aligned}
V^{(4)}_{m,4}(\mathbf{p},\mathbf{q};\mathbf{R}) = \frac{2}{(a_1^2+b_1^2)(c_4^2+d_4^2)}\big[c_4\big(\big[\varepsilon_n^2+I^2-\varepsilon(\mathbf{p})\varepsilon(\mathbf{p}+\mathbf{Q}_0+\mathbf{q})-\Delta_{\mathbf{p}}(\mathbf{R})\Delta^*_{\mathbf{p}+\mathbf{Q}_0+\mathbf{q}}(\mathbf{R})\big]\\
\times\big[\varepsilon_n^2-I^2-\varepsilon(\mathbf{p})\varepsilon(\mathbf{p}+\mathbf{Q}_0+\mathbf{q})-\Delta_{\mathbf{p}}(\mathbf{R})\Delta^*_{\mathbf{p}+\mathbf{Q}_0+\mathbf{q}}(\mathbf{R})\big]-\varepsilon_n^2\{[\varepsilon(\mathbf{p})+\varepsilon(\mathbf{p}+\mathbf{Q}_0+\mathbf{q})]^2\\
+|\Delta_{\mathbf{p}}(\mathbf{R})+\Delta_{\mathbf{p}+\mathbf{Q}_0+\mathbf{q}}(\mathbf{R})|^2\}+I^2[\varepsilon(\mathbf{p})^2-\varepsilon(\mathbf{p}+\mathbf{Q}_0+\mathbf{q})^2+|\Delta_{\mathbf{p}}(\mathbf{R})|^2-|\Delta_{\mathbf{p}+\mathbf{Q}_0+\mathbf{q}}(\mathbf{R})|^2]\\
-|\Delta_{\mathbf{p}}(\mathbf{R})\varepsilon(\mathbf{p}+\mathbf{Q}_0+\mathbf{q})-\Delta_{\mathbf{p}+\mathbf{Q}_0+\mathbf{q}}(\mathbf{R})\varepsilon(\mathbf{p})|^2\big)\\
+d_4b_1\big[\varepsilon_n^2+I^2-\varepsilon(\mathbf{p})^2-2\varepsilon(\mathbf{p})\varepsilon(\mathbf{p}+\mathbf{Q}_0+\mathbf{q})-|\Delta_{\mathbf{p}}(\mathbf{R})+\Delta_{\mathbf{p}+\mathbf{Q}_0+\mathbf{q}}(\mathbf{R})|^2+|\Delta_{\mathbf{p}+\mathbf{Q}_0+\mathbf{q}}(\mathbf{R})|^2\big]\big],
\end{aligned}
$$

$$
\begin{aligned}
V^{(4)}_{m,5}(\mathbf{p},\mathbf{q};\mathbf{R}) = \frac{2}{(a_1^2+b_1^2)(a_2^2+b_1^2)}\big(\big[\varepsilon_n^2-I^2-\varepsilon(\mathbf{p})\varepsilon(\mathbf{p}+\mathbf{Q}_0+\mathbf{q})-\Delta_{\mathbf{p}}(\mathbf{R})\Delta^*_{\mathbf{p}+\mathbf{Q}_0+\mathbf{q}}(\mathbf{R})\big]^2+b_1^2\\
-\big(\varepsilon_n^2+I^2\big)\{[\varepsilon(\mathbf{p})+\varepsilon(\mathbf{p}+\mathbf{Q}_0+\mathbf{q})]^2+|\Delta_{\mathbf{p}}(\mathbf{R})+\Delta_{\mathbf{p}+\mathbf{Q}_0+\mathbf{q}}(\mathbf{R})|^2\}\\
-|\Delta_{\mathbf{p}}(\mathbf{R})\varepsilon(\mathbf{p}+\mathbf{Q}_0+\mathbf{q})-\Delta_{\mathbf{p}+\mathbf{Q}_0+\mathbf{q}}(\mathbf{R})\varepsilon(\mathbf{p})|^2\big)
\end{aligned}
$$

with

$$
\begin{aligned}
&a_2=\varepsilon_n^2+\varepsilon(\mathbf{p}+\mathbf{Q}_0+\mathbf{q})^2+|\Delta_{\mathbf{p}+\mathbf{Q}_0+\mathbf{q}}(\mathbf{R})|^2-I^2,\\
&c_1=a_1a_2+b_1^2,\quad d_1=b_1(a_2-a_1),\\
&c_2=a_1a_2-b_1^2,\quad d_2=b_1(a_1+a_2),\\
&c_3=a_1^2-b_1^2,\quad d_3=2a_1b_1,\\
&c_4=a_2^2-b_1^2,\quad d_4=2a_2b_1.
\end{aligned}
\tag{A3}
$$

Here, we assume the Q2D Fermi surface distorted along the c direction. It leads to an incommensurate wave vector of the AFM order directed to [1,1,0] in the $\mathbf{H} \parallel ab$ case.

[1] P. Fulde and R. A. Ferrell, Phys. Rev. **135**, A550 (1964).
[2] A. I. Larkin and Yu. N. Ovchinnikov, Zh. Eksp. Teor. Fiz. **47**, 1136 (1964) [Sov. Phys.–JETP **20**, 762 (1965)].
[3] A. Bianchi, R. Movshovich, C. Capan, P. G. Pagliuso, and J. L. Sarrao, Phys. Rev. Lett. **91**, 187004 (2003).
[4] H. Adachi and R. Ikeda, Phys. Rev. B **68**, 184510 (2003).
[5] Y. Tokiwa, R. Movshovich, F. Ronning, E. D. Bauer, P. Papin, A. D. Bianchi, J. F. Rauscher, S. M. Kauzlarich, and Z. Fisk, Phys. Rev. Lett. **101**, 037001 (2008).
[6] Y. Tokiwa, R. Movshovich, F. Ronning, E. D. Bauer, A. D. Bianchi, Z. Fisk, and J. D. Thompson, Phys. Rev. B **82**, 220502(R) (2010).
[7] R. Ikeda, Phys. Rev. B **81**, 060510(R) (2010).
[8] K. Kumagai, H. Shishido, T. Shibauchi, and Y. Matsuda, Phys. Rev. Lett. **106**, 137004 (2011).
[9] R. Ikeda, Phys. Rev. B **76**, 134504 (2007).
[10] K. Kumagai, M. Saitoh, T. Oyaizu, Y. Furukawa, S. Takashima, M. Nohara, H. Takagi, and Y. Matsuda, Phys. Rev. Lett. **97**, 227002 (2006).
[11] M. Kenzelmann, Th. Strassle, C. Niedermayer, M. Sigrist, B. Padmanabhan, M. Zolliker, A. D. Bianchi, R. Movshovich, E. D. Bauer, J. L. Sarrao, and J. D. Thompson, Science **321**, 1652 (2008).
[12] M. Kenzelmann, S. Gerber, N. Egetenmeyer, J. L. Gavilano, Th. Strassle, A. D. Bianchi, E. Ressouche, R. Movshovich, E. D. Bauer, J. L. Sarrao, and J. D. Thompson, Phys. Rev. Lett. **104**, 127001 (2010).
[13] R. Ikeda, Y. Hatakeyama, and K. Aoyama, Phys. Rev. B **82**, 060510(R) (2010).
[14] Y. Hatakeyama and R. Ikeda, Phys. Rev. B **83**, 224518 (2011).
[15] J. Paglione, M. A. Tanatar, D. G. Hawthorn, Etienne Boaknin, R. W. Hill, F. Ronning, M. Sutherland, L. Taillefer, C. Petrovic, and P. C. Canfield, Phys. Rev. Lett. **91**, 246405 (2003).
[16] S. Singh, C. Capan, M. Nicklas, M. Rams, A. Gladun, H. Lee, J. F. DiTusa, Z. Fisk, F. Steglich, and S. Wirth, Phys. Rev. Lett. **98**, 057001 (2007).
[17] F. Ronning, C. Capan, A. Bianchi, R. Movshovich, A. Lacerda, M. F. Hundley, J. D. Thompson, P. G. Pagliuso, and J. L. Sarrao, Phys. Rev. B **71**, 104528 (2005).
[18] T. Park, Y. Tokiwa, F. Ronning, H. Lee, E. D. Bauer, R. Movshovich, and J. D. Thompson, Phys. Status Solidi B **247**, 553 (2010).
[19] F. Honda, R. Settai, D. Aoki, Y. Haga, T. D. Matsuda, N. Tateiwa, S. Ikeda, Y. Homma, H. Sakai, Y. Shiokawa, E. Yamamoto, A. Nakamura, and Y. Onuki, J. Phys. Soc. Jpn., Suppl. A **77**, 339 (2008).
[20] V. H. Tran, D. Kaczorowski, R. T. Khan, and E. Bauer, Phys. Rev. B **83**, 064504 (2011).
[21] R. Konno and K. Ueda, Phys. Rev. B **40**, 4329 (1989).
[22] M. Kato and K. Machida, Phys. Rev. B **37**, 1510 (1988).
[23] Y. Yanase and M. Sigrist, J. Phys. Soc. Jpn. **78**, 114715 (2009).
[24] K. M. Suzuki, M. Ichioka, and K. Machida, Phys. Rev. B **83**, 140503(R) (2011).

[25] Y. Kato, C. D. Batista, and I. Vekhter, Phys. Rev. Lett. **107**, 096401 (2011).
[26] N. Hiasa and R. Ikeda, Phys. Rev. Lett. **101**, 027001 (2008).
[27] E. Blackburn, P. Das, M. R. Eskildsen, E. M. Forgan, M. Laver, C. Niedermayer, C. Petrovic, and J. S. White, Phys. Rev. Lett. **105**, 187001 (2010).
[28] V. F. Correa, T. P. Murphy, C. Martin, K. M. Purcell, E. C. Palm, G. M. Schmiedeshoff, J. C. Cooley, and S. W. Tozer, Phys. Rev. Lett. **98**, 087001 (2007).
[29] X. Gratens, L. Mendonca-Ferreira, Y. Kopelevich, N. F. Oliveira, Jr., R. R. Urbano, R. A. Ribeiro, R. Movshovich, J. L. Sarrao, J. D. Thompson, Z. Fisk, and P. G. Pagliuso, Phys. Rev. B **85**, 054502 (2012).
[30] K. Kumagai (unpublished); K. Kumagai, H. Shishido, T. Shibauchi, and Y. Matsuda (unpublished).
[31] Y. Kasahara, Y. Nakajima, K. Izawa, Y. Matsuda, K. Behnia, H. Shishido, R. Settai, and Y. Onuki, Phys. Rev. B **72**, 214515(R) (2005).
[32] K. Aoyama and R. Ikeda, Phys. Rev. B **84**, 184516 (2011).
[33] C. Petrovic, R. Movshovich, M. Jaime, P. G. Pagliuso, M. F. Hundley, J. L. Sarrao, Z. Fisk, and J. D. Thompson, Europhys. Lett. **53**, 354 (2001).
[34] R. Ikeda, Phys. Rev. B **76**, 054517 (2007).
[35] In contrast, if the anisotropy of the Q2D material is large enough, the PPB-induced modulation of the SC order parameter is inevitably reflected in changes of the vortex lattice structure. As examples of such PPB-induced changes of the vortex lattice structure, see U. Klein, Phys. Rev. B **69**, 134518 (2004); N. Hiasa, T. Saiki, and R. Ikeda, *ibid.* **80**, 014501 (2009).
[36] G. Eilenberger, Z. Phys. **182**, 427 (1965).